Single-molecule studies of conformational states and dynamics in the ABC importer OpuA

Konstantinos Tassis[1,#], Ruslan Vietrov[1,2,#], Matthijs de Koning[1], Marijn de Boer[1], Giorgos Gouridis[1,3,4,*] and Thorben Cordes[1,5,*]

1 Molecular Microscopy Research Group, Zernike Institute for Advanced Materials, University of Groningen, Nijenborgh 4, 9747 AG Groningen, The Netherlands

2 Department of Biochemistry, Groningen Biomolecular Science and Biotechnology Institute, Netherlands Proteomics Centre & Zernike Institute for Advanced Materials, University of Groningen, Nijenborgh 4, 9747 AG Groningen, The Netherlands

3 Laboratory of Molecular Bacteriology, Department of Microbiology and Immunology, Rega Institute for Medical Research, KU Leuven, 3000 Leuven, Belgium

4 Structural Biology Division, Institute of Molecular Biology and Biotechnology (IMBB-FORTH), Nikolaou Plastira 100, Heraklion-Crete, Greece

5 Physical and Synthetic Biology, Faculty of Biology, Großhadernerstr. 2-4, Ludwig-Maximilians-Universität München, 82152 Martinsried, Germany

[#] these authors contributed equally to this publication

*corresponding author emails: g.gouridis@imbb.forth.gr, cordes@bio.lmu.de

Keywords: Single-molecule studies, membrane transport, ABC transporter, OpuA, glycine betaine transport, osmoregulation, substrate-binding domain, Förster-resonance energy transfer, conformational dynamics

Abstract: The current model of active transport via ABC importers is mostly based on structural, biochemical and genetic data. We here establish single-molecule Förster-resonance energy transfer (smFRET) assays to monitor the conformational states and heterogeneity of the type-I ABC importer OpuA from *Lactococcus lactis*. Our studies include intradomain assays that elucidate conformational changes within the substrate-binding domain (SBD) OpuAC and interdomain assays between SBDs or transmembrane domains. Using the methodology, we studied ligand-binding mechanisms as well as ATP and glycine betaine dependences of conformational changes. Our study expands the scope of smFRET investigations towards a class of so far unstudied ABC importers, and paves the way for a full understanding of their transport cycle in the future.

Introduction

ATP-binding cassette (ABC) transporters represent the most abundant and diverse family of transport proteins known. They play crucial roles in numerous cellular processes including nutrient uptake[1], antibiotic and drug resistance[2], antigen presentation[3], cell-volume regulation[4] and others[5-9]. Despite their importance, the majority of molecular models proposed for transport are based on the functional interpretation of static crystal structures, due to the inability of classical biophysical and biochemical techniques to visualize dynamic structural changes[5-9]. Advanced mechanistic insights, i.e., knowledge on structural dynamics and heterogeneity of conformational states in transporters, could be beneficial for the fight against pathogenic bacteria [10], and for the treatment of ABC related diseases such as cystic fibrosis[11] or multi-drug resistance in cancer cells[2]. Retrieving structural dynamics of drug targets allows to rationally design high-affinity drugs and understand the means by which drugs affect biological outcomes[12]. However, adapting a membrane-embedded biological system for complex biophysical investigations represent a huge bottleneck.

Over the past years[13], various labs have introduced single-molecule tools to decipher the structural dynamics of active membrane transporters[14-25]. In that respect, Förster resonance energy transfer in combination with single-molecule detection (smFRET[26-28]) has been proven a particularly useful tool for the validation of structural models[29-31] and for uncovering new mechanistic aspects, such as conformational heterogeneity[28, 32-34]. While the labs of Shimon Weiss[14], Scott Blanchard[15-17] and Antoine van Oijen[18] have published the first smFRET studies of secondary active transporters in a detergent environment[14-16] or within liposomes[17, 18], we introduced smFRET for studies of different ABC transporters in collaboration with the groups of Bert Poolman, Konstantinos Beis and Robert Tampé. These included importers (GlnPQ[19, 20]), their substrate binding proteins or domains[21], the ABC exporter McjD[23], and the non-transporting ABC-protein ABCE1[35]. Lewinsson[24] and Slotboom[36] have further performed detailed smFRET studies on the type-II ABC importer BtuCD-F. Also the influence of different membrane mimics (detergent, lipid nanodiscs and proteoliposomes) was presented in a recent study on the ABC exporter MsbA[25]. Advances in the visualization of structural dynamics in transporters have also been furthered by other biophysical techniques such as high-speed AFM[37] and EPR[38, 39].

All these studies were motivated by the idea to resolve long-standing key questions in the transporter field. These include ligand binding mechanisms and aspects of substrate selectivity in transport. Furthermore, the precise timescales of the conformational changes in transmembrane and nucleotide binding domains are not clear. Additionally, mechanistic differences, e.g., the specific conformational state at resting conditions, must be clarified for the distinct type-I and type-II ABC importers. Furthermore, it remains an ultimate goal of researchers in the field to establish complete models of transport by deciphering the coordination of transport, ATPase activity and the associated conformational changes. This includes precise understanding of how substrate binding and ATP hydrolysis events are coupled and transmitted from one domain to another via conformational changes that finally drive substrate transport.

We here extend our smFRET work on ABC-transporters to the osmoregulator OpuA. This ABC importer represents a well-established model system of type-I ABC transporters and is involved in cell volume regulation via the uptake of glycine betaine [4, 40]. It senses the intracellular ionic strength via two cytosolic domains (Cystathionine β-Synthase; CBS), which are attached to the nucleotide binding domains (NDBs)[4]. The CBS domains in conjunction with an anionic membrane surface, gate the transporter in response to osmotic stress for import of glycine betaine. OpuA is a paradigm for osmoregulatory ABC transporters and the system is widespread throughout the bacterial and archaeal kingdoms[4]. It is critical for the survival of low GC Gram-positive pathogens under conditions of

osmotic stress, but also plays an important role in osmoregulation in Gram-negative pathogenic bacteria[4].

The molecular architecture of OpuA is closely related to other type-I importer systems. The general domain organization of the transporter is shown in Figure 1a. Poolman and co-workers showed that OpuA is slightly more complex than other type-I ABC importers (e.g., the molybdate or maltose permease)[4, 40]. Each homo-dimer of OpuA consists of two different types of polypeptides per protomer. One encoding for the TMD and SBD (OpuABC), while the second OpuAA includes the NBDs and tandem CBS domains (Figure 1). A peculiarity of OpuA in comparison to the vast majority of type-I ABC importers, is the presence of the additional CBS domain, sensing the ionic strength of the environment [4, 40]. This distinctiveness might lead to a different mechanism of transport and/or its activation. For OpuA, the cycling of the NBDs from a dimeric ATP-bound state to a monomeric ADP-state is probably dependent on the CBS-CBS interaction, which is regulated by ionic strength and in particular potassium[4, 40, 41].

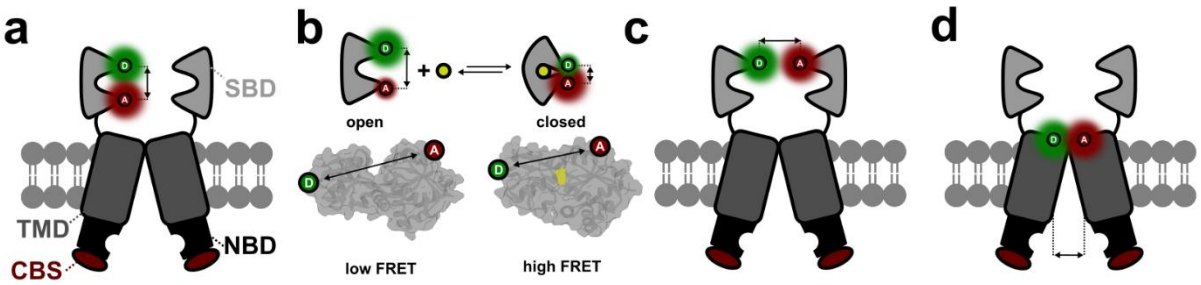

Figure 1. Setup for smFRET studies of the type-I ABC importer OpuA. **(a)** Structural organization of OpuA and intradomain FRET assay within the SBD. Please note that in our work also the second SBD can be labelled, yet these labels are not shown for simplicity in the scheme. **(b)** FRET assay principle to probe the conformational states of the SBD OpuAC via FRET. Open and closed structures are based on the published PBD structures of soluble OpuAC 3l6g and 3l6h, respectively, showing cysteine variant OpuAC (367C/423C) and ligand in yellow. **(c/d)** Interdomain FRET assays based on **(c)** SBD and **(d)** TMD labelling. Reactive coordinates probed in each panel are indicated by arrows and dashed lines.

Despite a more complex structure and gating of transport by ionic strength, OpuA is a suitable model system to derive the general principles of transport used by type-I importers via biophysical investigations on purified and *in vitro* reconstituted OpuA. Its activity can be tuned *in vitro* or *in vivo* via changes in the lipid composition used in the reconstitution reaction[4, 40, 41]. Importantly, OpuA is fully functional in bilayer nanodiscs, i.e., it shows a substrate-dependent ATPase activity with a high coupling efficiency and ionic-gating of activity, provided that a physiologically relevant lipid composition is used[40]. These achievements make the system suitable for single-molecule analysis and in particular for smFRET on diffusing molecules via confocal microscopy[19-21, 23], since membrane proteins reconstituted in lipid nanodiscs behave similarly to soluble proteins.

In this paper, we introduce the design and experimental realization of smFRET assays for OpuA. The studies aim to monitor various aspects of the OpuA conformational dynamics and to uncover structural heterogeneity (Figure 1). These include intradomain experiments to elucidate conformational changes within the SBD OpuAC in isolation, or in the context of the full transporter via smFRET (Figure 1a/b). Furthermore, we used smFRET to study interdomain interactions between SBDs (Figure 1c) and started to characterize the conformational states of the TMDs (Figure 1d). For this, we isolated and biochemically characterized various OpuA cysteine derivatives. Our results reveal a very similar ligand-binding behaviour of the extra-cellular binding domain OpuAC when the isolated protein

(Figure 1b) is compared to the transporter-linked one (Figure 1a). This relates to both its ligand affinity and the ligand-binding mechanism, which supports the relevance of mechanistic studies based on SBDs and SBPs in isolation (as done previously for various ABC-related SBPs/SBDs[21]). We further investigated the SBD-SBD interactions in a ligand-free or ATP-bound or glycine-betaine-bound state. Our findings on the kinetics of conformational dynamics of OpuAC show rapid ligand release times, which we believe facilitates the high transport rates of glycine betaine via OpuA [42, 43]. Finally, for TMD studies, we had to account for the lack of structural information available to us. To overcome this, we relied on homology modelling of the TMD aiming to label the extremes of trans-membrane helices lying on either side of the membrane and generated a large-number of cysteine derivatives. In the paper, we describe our screening process to identify the optimal labelling positions for retained biochemical activity and high labelling efficiency. With the most appropriate labelled derivative, we provide preliminary smFRET data on OpuA's TMD.

Our study expands the scope of smFRET investigations towards an important class of so far unstudied type-I ABC importers and paves the way for a deep understanding of the full transport mechanism of OpuA and related transporters in future studies based on advances made here.

RESULTS

Over the past years we have studied the ligand-binding properties of substrate-binding proteins or domains and their implications for transport in ABC importers, i.e., mechanisms related to ligand selectivity and the determination of the rate limiting steps in transport[19, 21, 44]. To link our previous investigations to the studies of the full-length OpuA transporter, we first asked the question whether the tethering of OpuAC to the TMD has a strong impact on its ligand binding behaviour. For this, we present a detailed comparison between isolated (Figure 1b) or membrane-tethered OpuAC domains (Figure 1a). To monitor the conformational states of OpuAC, i.e., the ligand-free open and ligand-bound closed (Figure 1b), we generated two double cysteine derivatives of OpuAC to probe conformational changes triggered upon ligand binding: OpuAC (360C-423C) also used in ref. [21] and OpuAC (367C-423C). Both mutations were located on the rigid domains of OpuAC and an increased proximity between the donor-and acceptor fluorophore is expected once OpuAC has bound the ligand (Figure 1b). The assay would thus indicate the OpuAC open state via a low FRET and the closed state via a high FRET efficiency state. In the attempt to maximize FRET-efficiency changes during conformational motion, possible interference of the cysteine residues and attached fluorophores with docking of the OpuAC in the transporter was initially not considered.

Conformational dynamics of the SBD OpuAC. To characterize the conformational changes of soluble OpuAC, we used both alternating laser excitation (ALEX) on diffusing molecules and confocal scanning microscopy of surface-immobilized ones[21]. We find that in line with previously published results, OpuAC (360C-423C) changes its conformation in a ligand-dependent fashion (Figure 2a/b). Both the open-unliganded (low FRET) and closed-liganded states (high FRET) are detectable and their occupancy changes according to the glycine betaine concentration in the buffer solution (Figure 2a/b). In the absence of glycine betaine, we find exclusively occupation of the open state (Figure 2a/b – apo), as was also shown previously[21]. This result and its interpretation are valid for freely diffusing (Figure 2a) and surface-immobilized OpuAC (Figure 2b). Identical results were obtained when an alternative pair of fluorophores was used for labelling (Alexa555/Alexa647, Figure S1). This suggests that the fluorophores do not compromise the conformational changes of OpuAC and do not alter the ligand

binding affinity. The supporting data in Figure S1 also shows the two-dimensional character of the ALEX experiments, i.e., low stoichiometry acceptor-only molecules (S < 0.3), intermediate stoichiometry donor-acceptor-labelled molecules (0.3 < S < 0.8) and high stoichiometry donor-only molecules (S > 0.8). For histograms shown in Figure 2a and subsequent figures where 1D-E* histograms are presented, we focussed on the analysis of the FRET-efficiency distributions in the intermediate stoichiometry region, where the protein carries one donor- and one acceptor fluorophore.

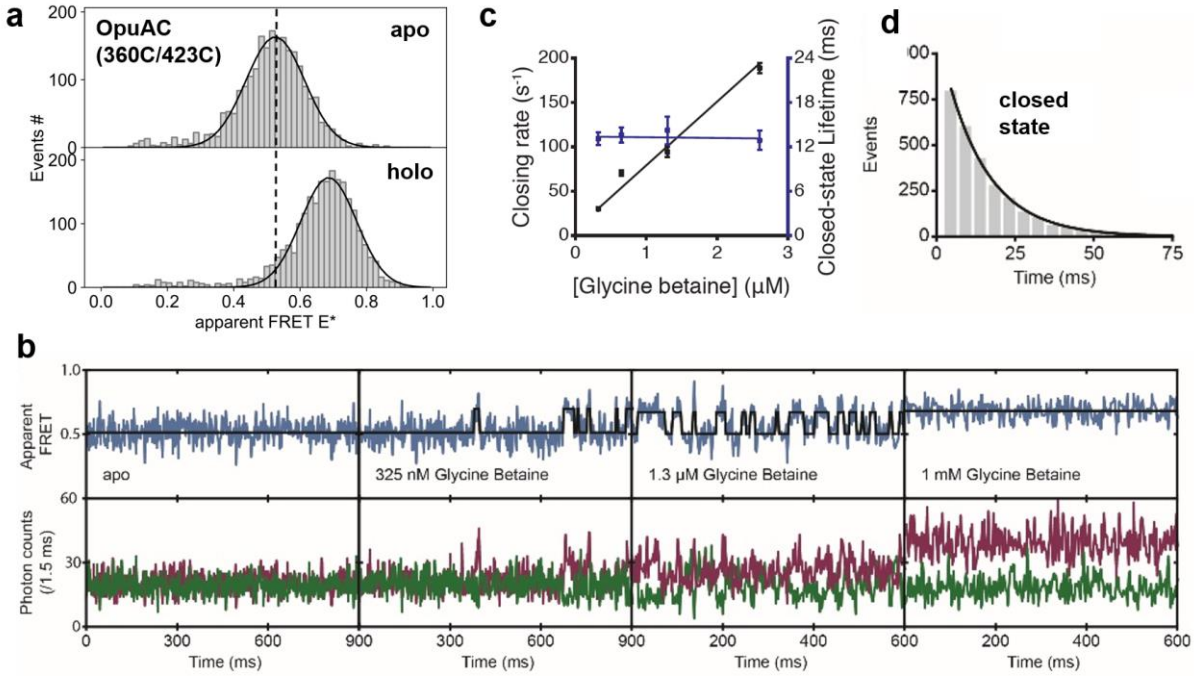

Figure 2. smFRET studies of isolated OpuAC (360C-423C) with Cy3B/ATTO647N as donor and acceptor fluorophore. **(a)** Apparent FRET efficiency histogram of freely diffusing fluorophore-labelled OpuAC molecules, obtained from the solution-based smFRET and ALEX measurements under the indicated conditions. **(b)** Fluorescence trajectories of OpuAC under different conditions as indicated; donor (green) and acceptor (red) photon counts are binned with 1.5 ms. The top panel shows calculated apparent FRET efficiency (blue) with the most probable state-trajectory of Hidden Markov Model (HMM) (black). **(c)** Average closing rate (black) and lifetime of the closed-state (purple) as function of glycine betaine concentration. Error bars indicate the 95% confidence interval. **(d)** Lifetime distribution of the closed state as obtained from the most probable state-trajectory of the HMM of all molecules. Grey bars are the binned data and the solid line is an exponential fit.

Next, we studied the dynamic conversion between both conformational states (Figure 2c). For this, the temporal evolution of donor- and acceptor signals of surface-immobilized OpuAC molecules were followed using confocal scanning microscopy. The FRET efficiency time traces show frequent switching between the low and high FRET state, which indicates the opening and closing transitions of OpuAC (Figure 2b). To obtain the associated kinetics, the time traces were fitted with a two-state hidden Markov model (HMM). The lifetime distributions of the low and high FRET states were obtained from the fit (as described in ref. [21], Figure 2c/d). From this, we extracted the average opening and closing rates (Figure 2c/d). We observe that the average openings rate is largely concentration independent, whereas the average closing rate scales approximately linearly with glycine betaine concentration. This ligand dependency is indicative of an induced-fit ligand-binding mechanism[19-21, 23], yet the limited time-resolution of 1.5 ms cannot rule out faster conformational switching in any of the conditions displayed. We have to stress, however, that the fluorescent time traces of OpuAC (360C/423C) are of very good quality and OpuAC has so far the fastest ligand-release time that we could still detect with HHM-analysis and dwell-time analysis amongst all SBPs and SBDs that we have

analysed so far[21]. Our data as a function of ligand concentration (Figure 2c) also suggest that the ligand-binding affinity (K_d) is in the low micromolar range, which we verified as shown below by detailed titration experiments. This ligand affinity is in line with the ones from published bulk experiments where K_d-values of ~4 µM were determined[45].

Conformational states and dynamics of soluble and membrane-anchored OpuAC. In order to quantify the ligand affinity of free OpuAC, in comparison to the physiological situation, where the protein is covalently tethered to the OpuA translocator (TMDs), we performed a glycine betaine titration (Figure 3). For this, we used OpuAC (367C-423C) with a slightly altered labelling scheme as compared to the data presented in Figure 2, i.e., OpuAC (360C-423C). The results are qualitatively similar and only the absolute FRET efficiencies are distinct between both experiments (compare apo/holo in Figure 2a and Figure 3a) due to differences in the inter-cysteine distance of both pairs. By fitting the FRET efficiency histograms with two Gaussian distributions, the relative population of the open and closed state was obtained as function of glycine betaine concentration [GB] (Figure 3b). The data points were fit to the function $r_c = [GB]/(K_d + [GB])$, which results in a dissociation constant K_d of ~6 µM for free OpuAC (95% confidence interval); the fit is displayed as a black line in Figure 3b. In the equation r_c is the fraction of OpuAC in the closed state.

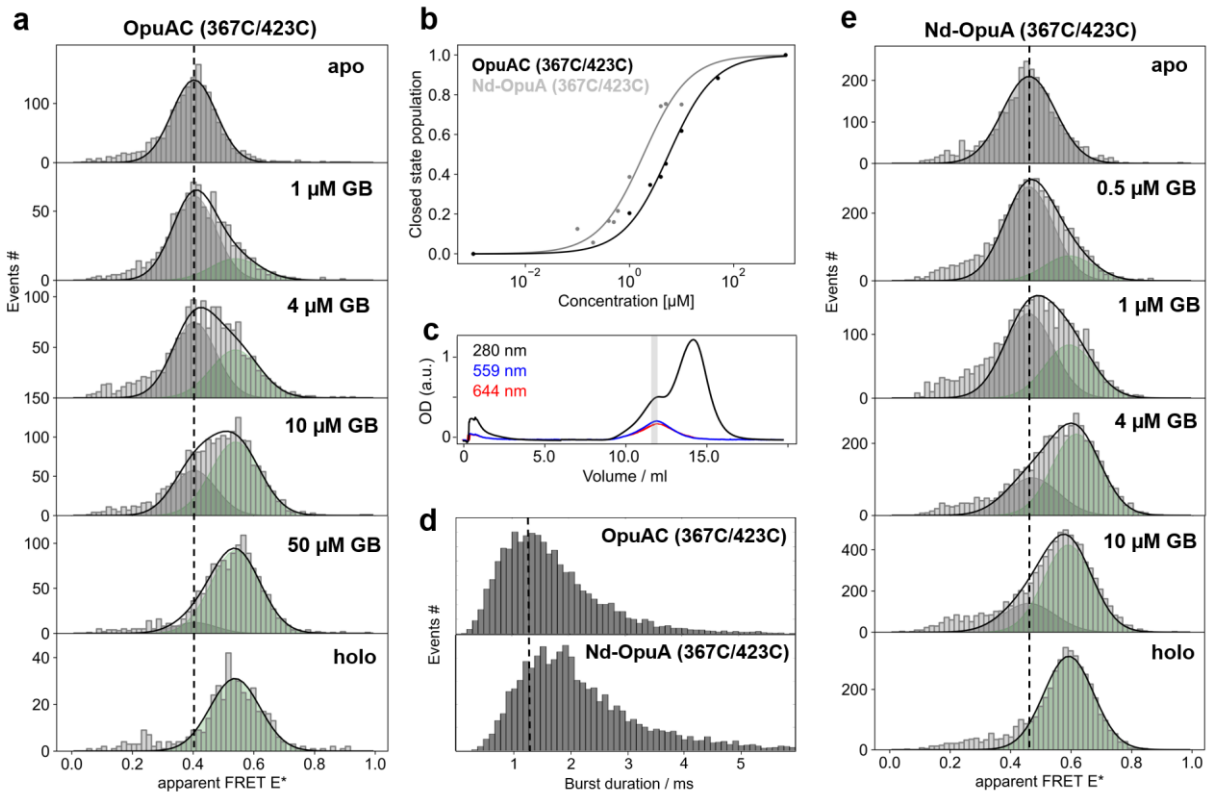

Figure 3. smFRET studies of intramolecular SBD conformation of free OpuAC (367C/423C) (a/b) or in the context of the transporter embedded in nanodiscs (c-e): Nd-OpuA (367C/423C). (a/e). Apparent FRET efficiency histogramof OpuAC / Nd-OpuA at different glycine betaine concentrations [GB] as indicated in the Figure. The relative populations of open/apo and holo/closed state were determined using a double-gaussian fitting model with a fixed mean and width and were plotted in **(b)** as a function of ligand concentration. **(c)** Size exclusion chromatogram of fluorophore labelled Nd-OpuA (367C/423C), light grey bar annotates the fraction used for the smFRET experiments. Examples of the full data sets are shown in Figure S2/S3. **(d)** Differences in burst duration, related to size increase in Nd-OpuA, were determined from the example data sets of panel **(a/e)**.

To study the conformational switching for OpuAC within the whole transporter, we reconstituted the corresponding cysteine variant of OpuA (367C/423C) into lipid bilayer nanodiscs using previously established protocols (details see Material and Methods)[40]. The experimental procedure is schematically sketched in Figure 4. In brief, OpuA derivatives were expressed and purified as described previously [40]. The cell pellets were disrupted by rounds of fractionation, membrane vesicles of *L. lactis* containing the overexpressed OpuA derivatives were isolated and stored (Figure 4, V). OpuA was solubilized by the use of DDM and immobilized on a Ni^{2+}-sepharose™ resin (Figure 4, I). Labelling with donor- and acceptor-fluorophores was performed at this stage. After removal of the excess of dyes, OpuA was reconstituted in lipid bilayer nanodiscs. The reconstituted material was further purified by Size-Exclusion Chromatography (SEC). Selected fractions of the SEC were analysed by SDS-PAGE to verify that the two non-covalently linked subunits of OpuA, OpuABC (TMD) and OpuAA (NBD) are not detached during the procedure (Figure S4) and remain active (Figure S5, wt OpuA). Proper biochemical activity was verified by assessing the glycine betaine and potassium-induced stimulation of ATPase activity, which was stimulated 4-10 fold over the basal level (Figure S5, wt OpuA).

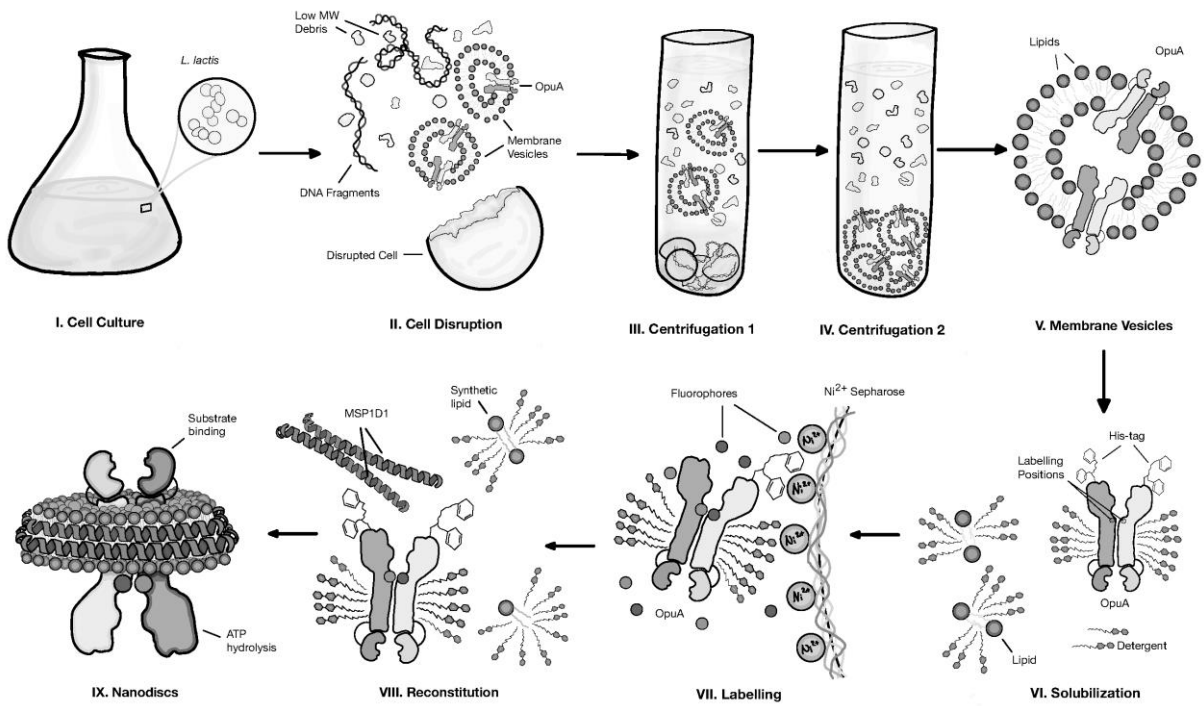

Figure 4. Workflow for smFRET studies of nanodisc-reconstituted OpuA. The OpuA cysteine derivatives (example used here refer to TMD positions) were overexpressed in *L. Lactis* (step I). The cells were mechanically ruptured (step II) and the protein-loaded membrane vesicle were isolated (steps III-IV). At this stage the membrane vesicles can be stored at -80°C until needed for a period of 6-12 months. OpuA was released from the membrane vesicles with a non-ionic detergent such as DDM (step VI). The solubilized transporter complex was then purified and labelled utilizing affinity chromatography (step VII). In the final step, OpuA was reconstituted into nanodiscs using synthetic lipids and an amphipathic scaffold protein MSP_1D_1 [46] (step VIII).

Using SEC-chromatography, we obtained a peak eluting at ~12 ml containing the reconstituted Nd-OpuA (367C/423C) derivative [40] and a second one with the empty nanodiscs at ~14 ml (Figure 3c). By determining the absorbance at the indicated wavelengths in the corresponding elution volumes (grey bar, Figure 3c), we estimated the labelling efficiencies, i.e., the relative concentration of donor-

and acceptor dye to OpuA (for details see methods parts below). As expected, from the size difference between free and nanodisc embedded OpuAC within the entire transporter, the nanodisc-reconstituted OpuA shows a slightly shifted burst-length distribution with respect to free OpuAC, indicating slower diffusion (Figure 3d).

Next, we investigated the smFRET histograms of the nanodisc-reconstituted Nd-OpuA (367C/423C) (Figure 3e) at different ligand concentrations, as was done for free OpuAC before (Figure 3a). OpuA can be labelled with more than 2 fluorophores in the 367C/423C variant, since four cysteines are present due to the fact that each protomer contains an OpuAC SBD. To exclude interdomain artefacts in our smFRET experiments, we analysed only molecules with a stoichiometry value >0.5 to bias our analysis towards OpuA-molecules bearing fewer fluorophores. This selection is based on the analysis of photon-counting histograms (Figure S3) of Nd-OpuA (367C/423C). From these the idea emerged that the acceptor-based acceptor-emission AA is lower in the high stoichiometry region, which suggests fewer acceptor labels here. Furthermore, low S molecules also show stronger donor-quenching, which is likely to be caused by the presence of multiple acceptor fluorophores.

In line with this interpretation and data selection, the resulting FRET efficiency histograms of soluble OpuAC and Nd-OpuA (367C/423C) were very similar. In addition, the fit of the glycine betaine response suggests a K_d value of ~2 µM for Nd-OpuA (367C/423C) (Figure 3b, grey fit line), which seems 3-fold higher as compared to the soluble OpuAC. This difference in K_d can be seen by distinct ratios of open/closed-state population at similar concentrations of glycine betaine (Figure 3a vs. Figure 3e). We can thus conclude that the conformational changes of OpuAC and ligand binding are only marginally influenced by its linkage with the translocator domain of OpuA.

In type-I ABC importers, TMDs are known to transit from the inward-facing state ("resting", free or ADP-bound), to the outward-facing ATP-bound state during transport [47]. To monitor whether these conformational changes are transmitted to the SBDs, we monitored the conformational states of OpuAC within the nanodisc embedded OpuA (Figure 5a, Figure S6).

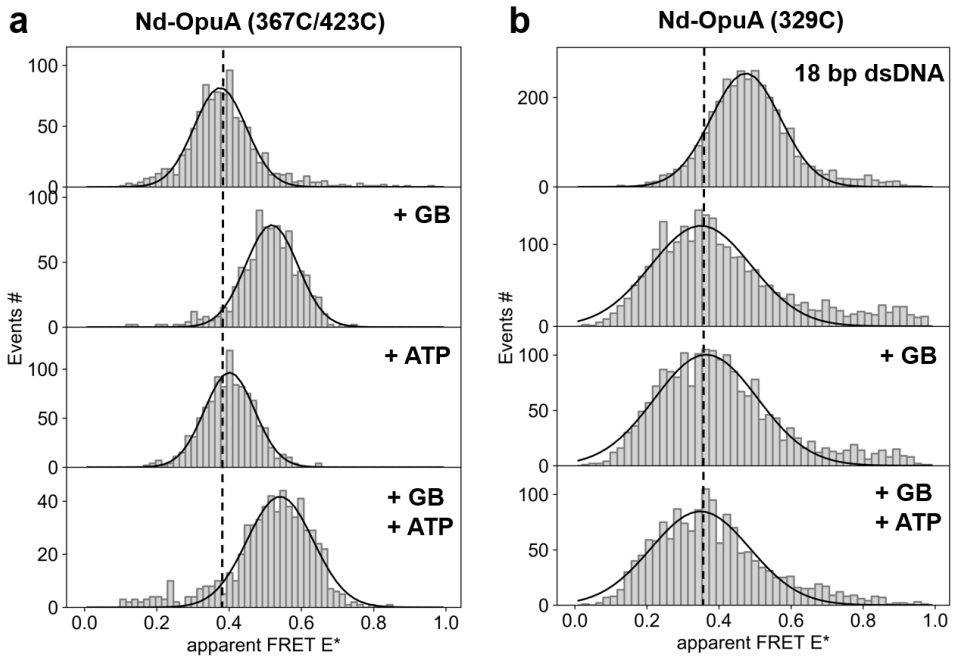

Figure 5. ATP- and ligand-dependent conformational switching of OpuA in nanodiscs with intramolecular SBD labels (**a**): **Nd-OpuA (367C-423C) and interdomain labels (b): Nd-OpuA (329C)**.

Our data suggest that addition of ATP does not influence the conformational state of OpuAC neither in the absence nor the presence of glycine betaine, using variant Nd-OpuA (367C/423C) (Figure 5a). Note that we assume here that ATP-hydrolysis is slow at room-temperature and can be used to induce conformational switching in ABC transporters using ALEX microscopy as shown previously for McjD[23]. This idea is supported by the fact that we obtained identical results as shown in Figure 5 (+ATP) with AMPPNP (data not shown). We thus conclude that the conformational changes of the TMDs driven by ATP binding are not transmitted to the SBDs in a way detectable by our FRET assay. However, we must note that the SBD-labelling scheme we used might impair the docking of OpuAC to the TMDs. Thus, future studies should focus on heterodimer expression of OpuA to avoid presence of more than one donor-acceptor pair and consider backside labelling of OpuAC to avoid such complications (see discussion for details).

The conformational arrangement of membrane-anchored SBDs. We next used the established fluorophore labelling procedure of nanodisc-reconstituted OpuA to study relative changes in interdomain distances between the two SBD domains within the full transporter (Figure 1c). For this, the labelling scheme was tailored to maintain only one cysteine per SBD and thus two per full transporter, i.e., Nd-OpuA (329C). The FRET efficiency histograms Nd-OpuA (329C) were obtained in the apo state or in the presence of glycine betaine and/or ATP (Figure 5b). The FRET-efficiency distributions were wider as compared to a static DNA sample with one defined distance or conformational state (Figure 5b). Similar observations were also made with another labelling position, i.e. Nd-OpuA (458C); data not shown. This suggests that either fast distance fluctuations occur on the sub-millisecond timescale or reveal the existence of multiple distances that give rise to overlapping distributions. To rationalize these interpretations, i.e., the existence of more than one possible structural state or a larger ensemble of states, we analysed a static DNA sample (Figure 5b, upper panel). Here, the donor-acceptor distance is 18 bp suggesting 6.1 nm distance between donor-acceptor attachment points using a linear DNA-model and 7.2 nm for cylindrical DNA model[48]. As was shown previously the width of such a distribution depends solely on photon statistics (and background) and is characteristic of a static conformational state[31, 49]. The broad and non-specific FRET-efficiency distributions of the interdomain labels in Nd-OpuA (329C) can also explain the lower data quality of Nd-OpuA (367C/423C) in comparison to soluble OpuAC (367C/423C). Nd-OpuA (367C/423C) showed a significantly elevated number of unspecific FRET events, which are likely related to interdomain FRET events and are found around the major population at E* ~ 0.4 of intramolecular FRET within OpuAC (see Figure S2, line 1 vs. line 2) due to the possibility of for labelling both SBDs.

Towards smFRET studies to probe the alternate access model. As high-resolution structures of the translocator domain (TMD) of OpuA were not available to us, we performed homology modelling by using the Swiss-Model server [50, 51] (Supplementary Note and Figure S7/8) to identify suitable positions and residues for smFRET studies of the TMDs of OpuA. The best templates for modelling were the structures of the bacterial importers for maltose (4jbw), molybdate tungstate (2onk), methionine (3dhw) and molybdate sulfate (3d31). Unfortunately, the sequence identity was <26% and the sequence similarity <32% suggesting that the resulting model may not be entirely accurate.

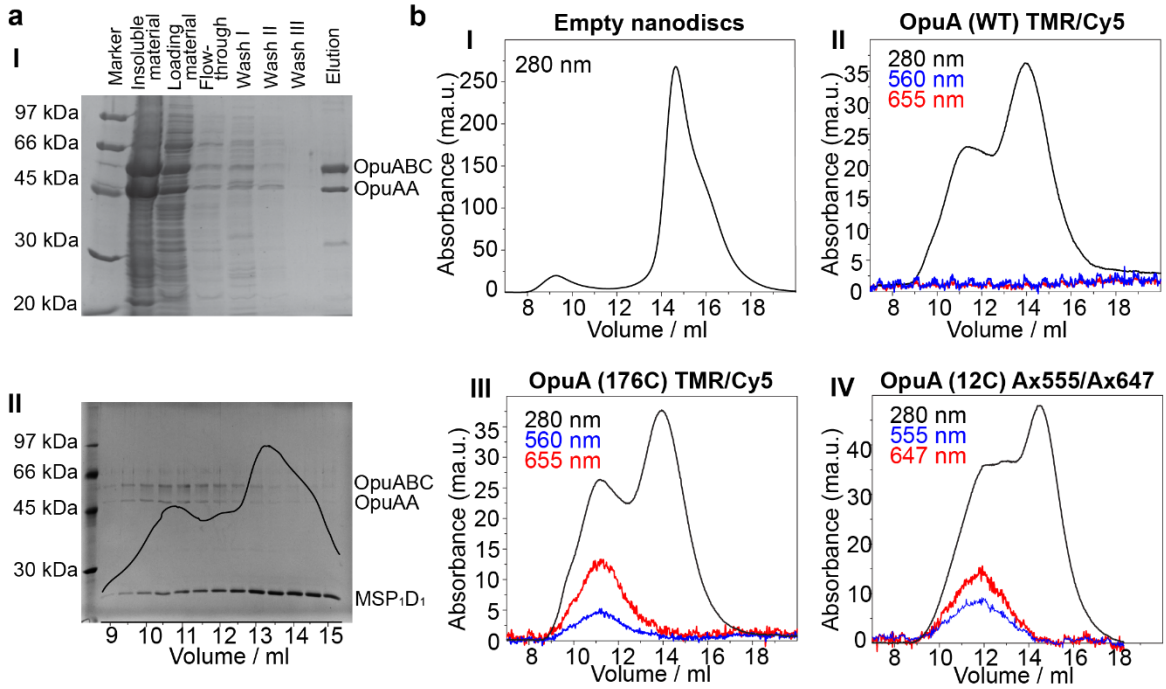

Figure 6. Optimization of fluorophore labelling for smFRET studies of OpuA TMD mutants. (a) SDS-PAGE of the purification process from membrane vesicles to detergent solubilized OpuA WT (I). SDS-PAGE analysis of the elution fractions of the reconstituted Nd-OpuA. The black line shows the size exclusion chromatogram and the correlation between SEC peaks and protein content (II). **(b)** Size exclusion chromatograms of (I) reconstituted nanodiscs without any OpuA. (II) Wild type OpuA reconstituted in nanodiscs and labelled with TMR and Cy5 to determine the absence of unspecific binding of the fluorophores to the cysteine-less Nd-OpuA. (III): Nd-OpuA 176C labelled with TMR and Cy5. (IV) Nd-OpuA 12C labelled with Alexa 555 and Alexa 647.

Keeping the limitations of the model and its unclear accuracy in mind, we focussed to establish an experimental pipeline to identify suitable TMD residues for smFRET with the goal to visualize changes between the inward- and outward facing conformation. As a first step we identified non-conserved residues that - according to our model - were surface exposed. Additionally, we set the conditions that those residues would need to undergo significant distance changes between the inward and outward facing conformation (Figure S7/8). As the two last points rely on the validity of our homology model, which we knew was questionable, we decided to generate a larger number of cysteine derivatives (Figure 6/7a). The translocator domain of OpuA is homodimeric, consequently we only needed to modify only one residue per protomer to obtain two anchor points for donor- and acceptor fluorophores. The resulting derivatives were subsequently tested for their *in vivo/vitro* functionality and labelling efficiency, as the ones residing at the extremes of transmembrane helices are not expected to compromise fluorophore attachment and transporter activity (Figure 7a).

The selected TMD-derivatives were labelled with different fluorophore pairs as exemplified in Figure 6 for Nd-OpuA (176C) with TMR/Cy5 and for Nd-OpuA (12C) with Alexa555/Alexa647. As seen in Figure 6, wildtype OpuA cannot be labelled with maleimide fluorophores due to absent thiol-groups (Figure 6). The labelling efficiencies were derived by monitoring the absorbance of the protein and the fluorescent dyes at their corresponding maximum wavelength. Concentration determination of protein and fluorophores was done via the Lambert-Beer law using published extinction coefficients (see methods section and Table S4), yet the contribution of MSP_1D_1 to the 280 nm absorbance could not be de-convoluted, since methods for this only became available quite recently [52]. The labelled fraction (~11-12 ml) expected to have the two OpuA components in equimolar ratio, was selected for subsequent testing in biochemical and biophysical assays (Figure 6b II).

a

OpuA TMD-Mutant	Relative in-vivo uptake (%); unlabeled	Relative in vitro ATPase assay (labelled, %)	Labelling Efficiency with TMR-Cy5 pair (%)	Relative distance change (Å)
Ala 12 Cys	63	70	39	10.7
Trp 14 Cys	61	43	27	10
Leu 102 Cys	60	46	4	8.4
Leu 106 Cys	66	96	7	10.5
Ile 110 Cys	83	120	7	8.3
Asn 176 Cys	84	16	49	8.4
Arg 180 Cys	130	25	43	10
Gln 181 Cys	98	13	18	9.7
Ser 183 Cys	117	48	30	14.4
Thr 184 Cys	89	28	41	12.4
Thr 196 Cys	0	8	81	12.3
Arg 198 Cys	5	-	-	12.8
Leu 244 Cys	8	-	-	14
Ala 245 Cys	105	49	37	7.9

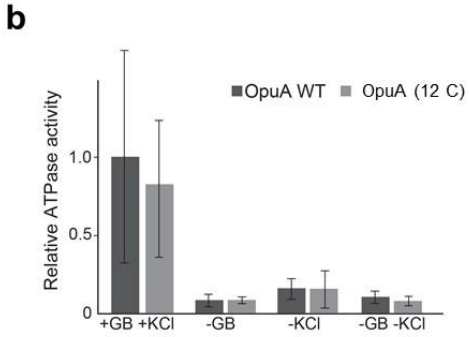

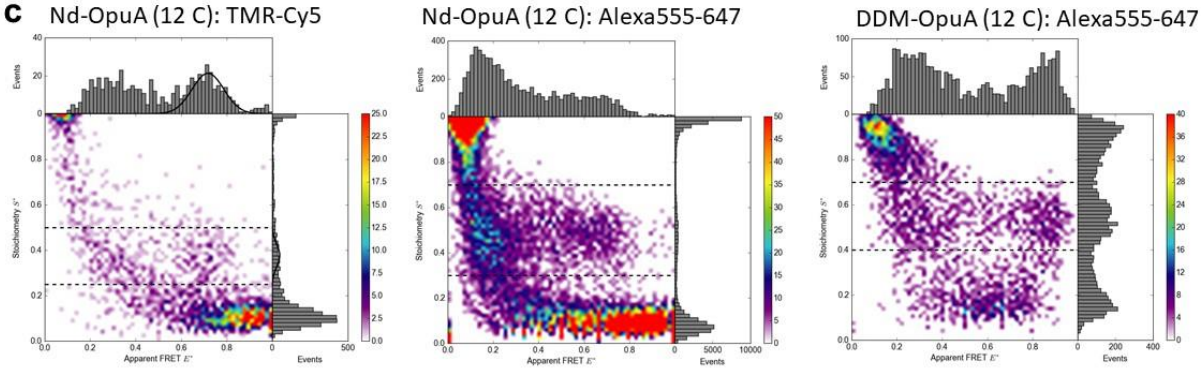

Figure 7. smFRET studies of TMD-labelled OpuA with OpuA (12C). (a) To select the appropriate cysteine derivatives for smFRET experiments we tested the effect of the cysteine point mutations and the fluorophore labelling to the activity of OpuA. Labelling efficiency is calculated by considering both donor and acceptor-labelling yields from SEC runs when comparing protein and dye absorbance. In the last column we also present the distance change between the modelled inward and outward conformation, an important parameter for the sensitivity of the smFRET assay. **(b)** ATPase activity comparison between labelled Nd-OpuA (12C) and OpuA WT; SEM is shown (N = 3). **(c)** Nd-OpuA (12C) with different fluorophore pairs showing increased donor-acceptor yield for use of Alexa555-647. For the data all photon burst-search was used (M = 15, T = 500 µs and L = 50) with additional thresholding of all photons >100. The S-range for 1D-E* histograms is indicated in the figure as dashed line.

To test the effect of the cysteine mutation on function, we first performed *in vivo* uptake assays using radiolabelled glycine betaine (Figure 7a) as described in ref. [40]. Moreover, to evaluate the effect of fluorophore attachment, we determined ATP hydrolysis rates for OpuA (12C) labelled with TMR-Cy5 pair in comparison to OpuA wildtype (Figure 7b). In Figure 7a, we summarize the relevant, substrate-stimulated ATPase activities in comparison to wildtype (100%); full data sets of different biochemical conditions (apo, KCl, GB and KCl) are shown in Supplementary Figure S6. We identified OpuA (12C) derivative as a promising candidate with a good degree of labelling efficiency (~40% total labelling efficiency of donor and acceptor dye) and well-retained function, which we believe was slightly compromised by cysteine introduction but not further by fluorophore attachment, for further smFRET studies (Figure 7c).

We performed ALEX experiments on the apo-protein state of OpuA (12C), i.e., ATP- and ligand-free conditions in both detergent and nanodiscs (Figure 7c). As the labelling efficiency was ~40% for TMR-Cy5, the donor-acceptor fraction is expected to be <10%. For that reason, in our preliminary ALEX experiments we observe a high degree of random coincidence, i.e., coincident detection of donor- and acceptor-only species due to elevated concentrations seen as a smear from low E/high S to low S values in this data set (Figure 7c, l-shaped lines between donor- and acceptor only at low FRET efficiency). For TMR-Cy5, however, there is a clear species at E* ~ 0.7, yet the presence of another low-FRET species,

which would be indicative of a second conformational state, cannot be ruled out due to the high level of random coincidence.

We next tried to use a commonly employed pair in smFRET Alexa555-647 and obtained labelling efficiencies of 39% in nanodiscs and 46% in detergent (Figure 7c). Despite the fact that a slightly higher donor-acceptor yield was found and that the fluorophores perform better in terms of brightness, Nd-OpuA (12C) labelling with Alexa dyes resulted in the appearance of two populations both in nanodisc and detergent. A peak in the low and intermediate FRET-regime could be indicative of two conformational states of the transporter related to changes of interresidue distance between 12C-labels, or artefactual interactions of the dyes with the protein. This example shows clearly that better data quality is required to clearly rule artefacts and also the availability of a high-resolution structure would be needed to interpret our results in a meaningful way.

DISCUSSION AND CONCLUSION

Long-distance allosteric communication dictates the function of both ABC importers[53] as well as ABC exporters[54]. The association and dissociation events of the NBDs that are driven by ATP binding and hydrolysis are transmitted to TMDs, which undergo conformational rearrangements that facilitate transport. SBDs act as primary receptors to bind and donate their respective substrates for transport initiation. The tight connectivity between the different domains is undisputed and its functional repercussions have been verified in many systems, e.g., the means by which the conformational changes of SBDs dictate substrate specificity[21] and transport[19]. However, many salient features of interdomain association remain elusive and represent the basis of distinction between the different transporter systems.

Substrate capturing by SBDs is the initial step for transport. In type-I systems, the SBDs acquire two distinct conformations, an open unliganded in which the two lobes are alike an open book and a closed liganded one, capturing the ligand by the well-known Venus fly trap motion[55]. Contrary, in type-II importers the structural rearrangements in the SBDs driven by the ligand are minor[55]. OpuAC from *L. lactis* is a type-I SBD linked to the TMDs. Thus, two OpuAC domains are present per functional transporter. In this paper, the SBD OpuAC was labelled with donor and acceptor fluorophores and its conformational states were probed by smFRET. Soluble OpuAC, as also previously reported for other members of the periplasmic binding protein family[21], binds its substrate by the Venus fly trap motion and most likely an induced fit mechanism according to our data. Its structural transitions are ligand dependent, and by titrating the ligand we derived K_d values via kinetic rate analysis and also occupation ratios of conformational states. Those are in excellent agreement with the ones determined in bulk, indicating that labeling and our smFRET assays do not interfere with ligand binding.

We also probed the conformational changes of OpuAC within the full transporter complex. For this, we tested many distinct labelling protocols including fluorophore addition (i) during the purification, (ii) solubilization or (iii) reconstitution of the entire transporter. The highest labeling efficiency was achieved when the fluorescent dyes were complemented to detergent-solubilized OpuA that was immobilized on the Ni-NTA column material (Figure 4). The 2D ALEX plot of the labeled OpuAC within OpuA indicate the existence of multiple labelling populations, as expected because of two OpuAC domains per transporter and the possibility of attachment of two fluorescent labels per OpuAC. With analysis based on fluorophore brightness (Figure S3) we can separate the populations (Figure 1a/3). The results indicate that OpuAC within the entire transporter obtains similar conformation states: open-unliganded and closed-liganded state. Furthermore, ligand titration indicates that OpuAC

within OpuA might have a slightly higher binding-affinity for glycine betaine. We must note that currently we cannot exclude that the labels hinder the docking process and further optimization of the labelling scheme is required to minimize this possibility.

The second step of transport is represented by the interaction of the SBD with the TMDs. In type-I importers, the TMDs differentiate between the open-unliganded or the closed-liganded state of the SBD. It is believed that interaction of the closed liganded state with the TMD [19] efficiently triggers ATP hydrolysis[42, 56]. Conversely, the ATPase activity of type-II importers can be ligand independent or shows at least much smaller stimulation values in the presence of liganded SBD/SBP[57, 58]. Such findings suggest a communication of the SBDs and the NBDs via the TMDs. Within our assays, we probed the OpuAC conformational states during transport conditions (glycine betaine + ATP) and throughout its resting state (apo). Addition of ATP and glycine betaine had no large effect on the conformational dynamics of OpuAC. Since a single SBD interacts with the TMD to deliver one substrate per transport cycle [42], an important question is whether the two OpuAC domains interact stochastically or in a concerted fashion with the TMD to release the substrate. To probe the relative movement of the two OpuAC domains, we placed one probe per domain. Our results indicate that probably, there are fast non-concerted motions between the two SBDs that are independent on the state of the TMDs. Future studies should reveal the relative motions of the two OpuAC domains during nucleotide cycling in more detail using advanced fluorescence methods with improved temporal resolution such as multi-parameter fluorescence detection (MFD analysis[30]), fluorescence correlation spectroscopy or pulsed-interleave excitation[49].

The absence of ATP/ligand-driven effects in our study might, however, also result from a failure of our labelled mutants to dock to the translocator TMDs due to steric hindrance effects and the chosen positions, which were only optimized for smFRET and not the biochemical activity. In future experiments, such effects must be avoided by use of alternative labelling schemes, e.g., on the back of OpuAC. Optimal labelling residues on the back of OpuAC (hinge region) for use of Cy3B/ATTO647N or Alexa555/647 would be A414C-A569C, A414C-A565C, A414C-A570C or A414C-A562C for intradomain monitoring (or any of these single cysteins for interdomain monitoring) considering the Förster radii of the two fluorophore pairs and the fact that they were used successfully for labelling nanodisc-reconstituted OpuA here.

The next step of transport involves the TMD conformational changes that needs to occur to promote the passage of the substrate to the cell interior. Those changes are assumed to be strongly coupled to the ATPase cycle in type-I importers [53]. Type-I ABC transporters switch from the resting state of the inward facing conformation to the outward, a process coupled to ATP and SBD binding events – which is distinct for type-II importers. That might be the reason that in type-I importers the ATPase activity is better regulated (i.e., here ATP hydrolysis is generally well coupled to translocation), whereas type-II manifest high basal ATPase activities in the absence of SBD and substrate. To probe transitions between the inward and outward facing conformation of OpuA, we produced a large number of cysteine derivatives to account for the lack of structural knowledge available to us. We started with a set of 14 mutants of which 11 still proved to be functional (>60% transport activity *in vivo*). Remarkably, while the chosen positions are surface-exposed according to our homology model, the majority could not be labeled well with dyes, suggesting that the position might be distinct from what is suggested in the model. The low sequence conservation of OpuA with available structures renders this finding not surprising. However, we selected the best derivative with respect to the labeling efficiency and the retention of the *in vivo* and *in vitro* functionality. The interpretations of the smFRET results of Nd-OpuA (12C) are still not fully clear since the resulting donor-acceptor yields were generally too low for in depth interpretation. Without further studies we cannot claim with confidence whether we observe one or multiple conformational states at this position and also whether the choice

of different fluorophore-pairs might have impacted our observations (Figure 7c). In the future more experiments with improvement of labelling efficiency and in particular donor-acceptor-containing functional transporter molecules are required. This type of problem, i.e., high obtained labelling efficiency yet low donor-acceptor fractions when labelling TMD-residues in ABC transporters, was reported by us [23] and others [24]. The problem was much less pronounced when the labelling was performed on the NBDs [23, 24]. Improvement of this aspect could reduce the measurement times from >1 hour for proper statistics, to shorter periods and would allow further testing of different biochemical studies of the transport cycles.

In summary, despite all problems encountered, we here pave the way for future experimental smFRET studies that aim at understanding the salient features of inter- and intra-domain communication in ABC transporters and in particular for OpuA.

METHODS

OpuA mutagenesis, expression and membrane vesicle isolation. The OpuA nucleotide sequence, (no endogenous cysteines), from *Lactococcus Lactis* was subcloned to the pBR322 vector (Addgene). The plasmid was used for the introduction of point cysteine mutations eligible for labelling by QC-PCR (Supplementary Table S3). The point mutants were subsequently cloned in the pNZopuAHis plasmid (C-terminal 6-HIS-tag) using *Eco*RV-*Alnwn*I (NEB) for the substrate-binding domain mutants and *Bam*HI-*Alwn*I (NEB) for the transmembrane domain mutants (Appendix). For the expression of the mutant proteins *L. lactis* Opu401 strain was used, which contains deletion of endogenous *OpuA* genes from the chromosome. 2-5-liter cultures were grown anaerobically at 30 ^{o}C in 2% (w/v) Gistex LS (Strik BV, Eemnes, The Netherlands) and 200 mM potassium phosphate (KPi), pH 7.4, supplemented with 1.0% (w/v) glucose and 5 μg/ml chloramphenicol. At OD_{600} ~2 the *nisA* promoter was induced by the addition of 1 ng/ml nisin. Two hours later the cells were harvested by centrifugation (6000 *g*; 15 minutes; 4°C) and stored at -20°. For the isolation of *L. lactis* membrane vesicles all handling was done at 4°C unless stated otherwise. The harvested pellet was resuspended in 50 mM KPi, 200 mM KCl, 20% glycerol, pH 7.4 (buffer A) in the presence of 1.5 mM dithiothreitol (DTT). To reduce the viscosity caused by the release of DNA, 100 μg/ml DNase and 2 mM MgSO4 were added. The suspension was disrupted through a continuous disruption cycle, twice at 40 Psi in a Constant Cell Disruption System LTD. In the disrupted material 1mM PMSF and 5mM EDTA, pH 8.0 was added. First, large cellular debris were removed by centrifugation (11,800 *g*; 20 minutes; 4°C) the pellet was discarded and the supernatant was centrifuged again (125,000 *g*; 60 minutes; 4°C). The pellet containing membrane vesicles was resuspended in buffer A and 1mM DTT and centrifuged again (125,000 *g*; 60 minutes; 4°C) to remove any remaining soluble components. The isolated membrane vesicles were resuspended in buffer A in the presence of 1mM DTT, aliquoted and flash frozen in liquid N_2 and then stored in -80°C. The total protein concentration was determined using the Pierce™ BCA Protein Assay Kit.

OpuA purification and labelling. All the handling described below was done at 4°C unless mentioned otherwise. The stored membrane vesicles were thawed and resuspended in buffer A (50 mM KPi, 200 mM KCl, 20% glycerol, pH 7.4) with the addition of 1 mM DTT and 10 mM *n*-Dodecyl β-D-maltoside (DDM) and incubated for 60 minutes while gently agitated. The solubilized protein was separated from any insolubilized material by centrifugation (267,000 *g*; 20 minutes; 4°C). The harvested supernatant was diluted with buffer A to a final DDM concentration of 2 mM and loaded to Ni^{2+}-Sepharose™ 6 fast flow resin (GE Healthcare, already equilibrated with 10 CV buffer A with 780 μM DDM) and was

incubated for 60 minutes under gentle agitation. The resin-bound material was washed three consecutive times (10 CV of each: buffer A with 1mM DTT and 780 µM DDM, buffer A with 1 mM DTT and 20 mM imidazole and 780 µM DDM, and buffer A with 1 mM DTT and 40 mM imidazole and 780 µM DDM) to remove all the weakly bound proteins. The purified protein was then eluted with buffer A with 200 mM imidazole and 780 µM DDM. For the labelling process the elution step was eschewed and the resin was drained and washed with buffer A and 780 µM DDM to remove DTT. Then 100 nmol of maleimide fluorophores (molar ratio of 7-10 fluorophores per cysteine available) were solubilized in 10 µl water-free dimethyl sulfoxide (DMSO) at room temperature and then suspended in buffer A and 780 µM DDM. The fluorophore mixture was added to the drained resin and incubated for 60min under gentle agitation. The excess of fluorophores was washed with 10 CV buffer A and 780 µM DDM and the labelled OpuA was eluted with buffer A, 200 mM imidazole, 780 µM DDM (Supplementary Figure S5b,c). The protein and fluorophore concentrations were estimated using Lambert-Beer's law ($A = \varepsilon lc$). The absorbance was calculated by measurements at 280 nm, 560 nm and 655 nm (calculating the area under the chromatogram of the relevant fraction). The path length was 0.1 cm and the extinction coefficients were available in the data sheets of the fluorophores (supplementary Table S4). Labelling efficiency was calculated as 100 x moles of total fluorophores / moles of cysteines. The purified OpuA was directly used for reconstitution into nanodiscs.

OpuA nanodisc formation and purification. An optimized synthetic lipid mixture dissolved in 50 mM KPi, pH 7.0 (50% 1,2-dioleoyl-sn-glycero-3-phosphoethanolamine, DOPE: 12% 1,2-dioleoyl-sn-glycero-3-phosphocholine, DOPC: 38% 1,2-dioleoyl-sn-glycero-3-phospho-(1'-rac-glycerol), DOPG, Avanti Polar Lipids) was prepared as described [40]. The lipid mixture was thawed and subsequently extruded through a 400 nm pore size polycarbonate filter, generating large unilamellar vesicles. 12 mM DDM was added and the mixture was vortexed until optically clear. The final reconstitution reaction was 50 mM KPi, 20% glycerol, 12 mM DDM and contained 1 nmol OpuA (labelled/unlabeled), 10 nmol MSP_1D_1, 1 µmol lipids in a final volume of 700 µl. To control for size and formation of nanodiscs, reconstitution reactions without OpuA were carried out and tested using size-exclusion chromatography (SEC). The reaction was incubated for 60 minutes at 4°C, while gently agitated. Then, 500 mg of SM2 bio-beads was added to the reaction volume and incubated for 1-12 hours with best result at 1-2 hours of incubation. The bio beads where removed and the solution was centrifuged (18000 *g*; 10 minutes; 4 °C) to precipitate any aggregated lipids and proteins. To determine the composition of the nanodiscs and to separate the nanodiscs from aggregates and empty nanodiscs, the supernatant from the previous step was purified using SEC, using a Superdex 200 10/300 GL column (GE Healthcare) that was previously equilibrated with 50 mM KPi, pH7.0, 200 mM KCl, 4% w/v glycerol buffer. The protein composition of the SEC fractions was verified by SDS-PAGE on 12% polyacrylamide gels.

MSP_1D_1 expression and purification. Membrane scaffold protein MSP_1D_1 was used for the formation of nanodiscs [40]. *E. coli* BL21(DE3) cells were freshly transformed with the $pMSP_1D_1$ plasmid and grown in 2 l Terrific Broth-kanamycin (10 µg/ml) medium at 37 °C under aerobic conditions. At OD_{600} of 1.5 the culture was induced with 1 mM isopropyl 1-thio-D-galactopyranoside (IPTG), three hours later the cells were harvested by centrifugation (8000 g; 20min; 4 °C). From this step onwards all the processes were done at 4°C and all solutions were at 4°C, unless stated otherwise. The cell pellet was re-suspended in 20 mM KPi, 1% Triton X-100, 1 mM PMSF at pH 7.4. The cells were lysed by sonification (5 sec on/ 5 sec off, 70% amplitude, 3 minutes). The cell lysate was fractionated by centrifugation (125000 g; 75 min; 4°C) and the pellet was discarded. Ni^{2+}-Sepharose™ 6 fast flow resin (GE Healthcare) was equilibrated with 10 column volumes of 40 mM KPi, pH 7.4 and the supernatant of the previous

centrifugation was gravity loaded to the column. The resin-bound MSP_1D_1 was sequentially washed with 10 column volumes of 40 mM Tris/HCl, 0.3 M NaCl, 1% Triton X-100, pH 8.0, then 40 mM Tris/HCl, 0.3 M NaCl, 50 mM sodium cholate, 20 mM imidazole, pH 8.0 and lastly with 40 mM Tris/HCl, 0.3 M NaCl, 50 mM imidazole, pH 8.0. MSP_1D_1 was then eluted with 40 mM Tris/HCl, 0.3 M NaCl, 0.4 M Imidazole, pH 8.0. The eluent was dialyzed overnight (SnakeSkin™ Dialysis Tubing, 7K MWCO ThermoFisher Scientific) against 20 mM Tris/HCl, 0.1 M NaCl, 0.5 mM EDTA, pH 7.4. Lastly, it was dialyzed once more overnight against 20 mM Tris/HCl, 0.1 M NaCl, 0.5 mM EDTA, 50% glycerol, pH 7.4. The protein concentration was calculated by absorbance at 280 nm (extinction coefficient 21,000 M^{-1} cm^{-1}; see Supplementary Figure S5a). The purified protein was aliquoted and stored at -20 °C.

ATPase activity assay. To determine the activity of the reconstituted OpuA, a coupled-enzyme activity assay was used to measure the ATPase activity of the reconstituted transporter. The coupled enzymatic reaction contained ~2 units of pyruvate kinase/lactic dehydrogenase (rabbit muscle isolate mixture, Sigma Aldrich) 50 mM KPi, pH 7.0, 300 mM NADH, 4 mM phosphoenolpyruvate (PEP), 62 µM Glycine Betaine, 300 mM KCl and 4 µg of OpuA reconstituted in nanodiscs. The change in absorbance at 340 nm was observed with a Synergy MX 96-well plate reader (Bio Tek Instruments, Inc.). The reaction components were incubated in the plate reader at 30 °C for 3min. Then 10 mM MgATP, pH 7.0, was added shaking the plate for 10 seconds to mix the compounds. A seven minute kinetic read (340 nm, 30 °C) with minimal time intervals was executed. The data were corrected for the path length of each individual reaction volume. For every mutant tested, controls were done in the absence of: a) glycine betaine, b) KCl, c) glycine betaine and KCl (Supplementary Figure S6). The ATPase activity was calculated from the slope of the measurements and normalized against the WT internal control.

Radiolabeled isotope uptake. For the in vivo radiolabeled-isotope uptake in *L. lactis* the previously published method was used [59]. Briefly, *L. lactis* Opu401 transformed with the appropriate plasmid was grown in glucose-CDM with 5 µg/mL chloramphenicol. At $OD_{600} \sim 0.5$ the culture was induced with 0.01% (v/v) nisin A (filter-sterilized culture supernatant from *L. lactis* NZ9700) until $OD_{600} \sim 1$. The cells were washed and resuspended at 2.5 mg of cell protein/ml in 50 mM HEPES-methylglucamine pH 7.3. Next, 10 mM glucose was added and the cells were incubated for 5 min at 30°C. To start the uptake a final concentration of 600 mM sucrose (osmotic stress to increase the internal ionic strength of the cell and activate OpuA), 1mM [^{14}C] glycine betaine in the presence and 50 µg/ml chloramphenicol (to prevent protein synthesis) were added to a reaction volume of 500 µl. 80 µl samples were taken at regular time intervals and diluted with 2 mL of ice-cold assay buffer of equal osmolality and filtered through 0.45 µm cellulose nitrate filters under high vacuum. The membranes were washed with ice cold 50 mM HEPES-methylglucamine pH 7.3. After drying, 2 ml of scintillating liquid was used to dissolve the membranes. The radioactivity was determined in a scintillation counter.

OpuA structure modelling. The homology model for the prediction for candidate mutagenic sites was done using Swiss Model Server [50, 51]. The template structure used were the molybdate/tungstate ABC transporter from *Archaeoglobus fulgidus* (ModBC, 2onk), the Maltose transport system from *Escherichia coli* (MalG, 2r6g and 4jbw), the molybdate/tungstate transporter from *Methanosarcina acetivorans* (ModBC, 3d31) and the methionine importer (MetNI, 3dhw). The sequence identity between OpuA and the templates was between 20.4% and 26.6 while similarity was ~30%. To calculate the relative distant change the produced model was aligned with the inward and outward facing conformations of the maltose transporter in PyMol [60] and the distances were measured also with PyMol for Ca-positions of the residues.

Solution smFRET measurements and data analysis. The methods and experimental devices used here have been described previously in detail [19, 20, 44, 61]. In brief, labelled OpuAC or OpuA was diluted to 20-100 pM in imaging buffer: 50mM potassium phosphate pH 7.4, 1mM Trolox and 10mM cysteamine (pH 7.5; Sigma-Aldrich). For this, the diluted protein was loaded to BSA (200 µl of 1 mg/ml for 30 seconds) treated coverslips (no. 1.5H precision cover slides, VWR Marienfeld), minimizing fluorophore interactions with the glass slide. The measurements were done using a custom-built confocal microscope[19, 20] at room temperature. Excitation was at 532 and 640 nm in accordance with the fluorophore absorbance maxima (SuperK Extreme, NKT Photonics, Denmark). Alternation between the two excitation wavelengths was achieved by 50 µs alternation. The output beam was coupled to a single-mode fiber (PM-S405-XP, Thorlabs, United Kingdom) and recollimated (MB06, Q-Optics/ Linos, Germany) before entering an oil immersion objective (60×, NA 1.35, UPLSAPO 60XO, Olympus, Germany). Excitation and emission were separated by a dichroic beam splitter (zt532/642rpc, AHF Analysentechnik, Germany) mounted in an inverse microscope body (IX71, Olympus, Germany). Fluorescence emitted by diffusing molecules in solution was collected by the same oil objective, focused onto a 50 nm pinhole and spectrally separated (640DCXR, AHF Analysentechnik, Germany) onto two APDs (τ-spad, < 50 dark counts/s, Picoquant, Germany) with the appropriate spectral filtering (donor channel: HC582/75; acceptor channel: Edge Basic 647LP; both AHF Analysentechnik, Germany). Unless mentioned otherwise in the figure legends ALEX data [23, 44] was analysed with a dual-colour burst search (M = 15, T = 500 µs and L = 25) and the resulting data were plotted with 61x61 bins considering an S-range of 0.3-0.8 with additional thresholding of all photons >100. The data of OpuA (A12C) were collected by a similar confocal microscopy setup as described in [44]. Here, the excitation was done via two Coherent Obis lasers centered at 532 and 637 nm and the objective lens was 60X, NA 1.2, UPlanSAPO 60XO (Olympus, NL).

Confocal scanning microscopy and data analysis. For surface immobilization of OpuA nanodiscs custom flow cells were made as previously described in [19, 23, 61]. The flow cell surface was functionalized at room temperature with a neutravidin solution; 0.2 mg/ml neutravidin (Invitrogen, United States) in 50 mM potassium phosphate pH 7.4, filtered with 250 µm syringe filter (buffer B) for 5-10 minutes. The unbound excess of neutravidin was washed with the same buffer. Subsequently, the surface of the flow cell was incubated with an anti-His antibody (in buffer B) for 5 minutes and washed again with buffer B. Then OpuAC was introduced to the flow cell (in buffer B supplemented with 10 mM of (±)6-Hydroxy-2,5,7,8-tetramethylchromane-2-carboxylic acid (Trolox; Merck) as a photostabilizer[20]) and incubated for 30-120 seconds while at the same time scanning the surface to determine the optimum density. When the particle density was adequate the excess of labelled proteins was washed away, using buffer B with 10 mM Trolox. Fluorescence traces were recorded at room temperature. The fluorescent trajectories were analysed using a hidden Markov Model[62] as described in [21]. The binning time was 1.5 ms.

ACKNOWLEGDEMENTS

This work was financed by an NWO Veni grant (722.012.012 to G.G.), an ERC Starting Grant (ERC-STG 638536 – SM-IMPORT to T.C.) and the Zernike Institute for Advanced Materials (support to G.G. and T.C.). G.G. also acknowledges an EMBO fellowship (long-term fellowship ALF 47-2012), and the Rega

Foundation postdoctoral program of KU Leuven. We thank J. Hammerl for preparation of Figure 4 and C. Gebhardt for providing data analysis scripts. We thank B. Poolman for continuous support of the project, which included conceptional discussions on the structure and function of OpuA and access to materials and protocols. We finally thank G. K. Schuurman-Wolters for experimental support and B. Poolman for critically reading the manuscript.

AUTHOR CONTRIBUTIONS

G.G. and T.C. conceived and designed the study and supervised the project. K.T., R.V., M.d.K and G.G., performed molecular biology and biochemistry studies. R.V. and G.G. developed the labelling protocols. K.T., R.V., M.d.B. and G.G. performed single-molecule experiments. K.T., M.d.B., G.G. and T.C. analysed data. K.T., G.G. and T.C. prepared figures and wrote the manuscript. All authors contributed to discussion of the research and approved the final version of the manuscript.

REFERENCES

1. Schuurman-Wolters, G. K. & Poolman, B. (2005) Substrate specificity and ionic regulation of GlnPQ from Lactococcus lactis. An ATP-binding cassette transporter with four extracytoplasmic substrate-binding domains, *J Biol Chem.* **280**, 23785-90.

2. Sharom, F. J. (2008) ABC multidrug transporters: structure, function and role in chemoresistance, *Pharmacogenomics.* **9**, 105-27.

3. Abele, R. & Tampe, R. (2004) The ABCs of immunology: structure and function of TAP, the transporter associated with antigen processing, *Physiology (Bethesda).* **19**, 216-24.

4. Biemans-Oldehinkel, E., Doeven, M. K. & Poolman, B. (2006) ABC transporter architecture and regulatory roles of accessory domains, *FEBS Lett.* **580**, 1023-35.

5. Davidson, A. L., Dassa, E., Orelle, C. & Chen, J. (2008) Structure, function, and evolution of bacterial ATP-binding cassette systems, *Microbiol Mol Biol Rev.* **72**, 317-64, table of contents.

6. Oldham, M. L., Davidson, A. L. & Chen, J. J. C. o. i. s. b. (2008) Structural insights into ABC transporter mechanism. **18**, 726-733.

7. Kos, V. & Ford, R. C. (2009) The ATP-binding cassette family: a structural perspective, *Cell Mol Life Sci.* **66**, 3111-26.

8. Parcej, D. & Tampe, R. (2010) ABC proteins in antigen translocation and viral inhibition, *Nat Chem Biol.* **6**, 572-80.

9. Locher, K. P. (2009) Review. Structure and mechanism of ATP-binding cassette transporters, *Philos Trans R Soc Lond B Biol Sci.* **364**, 239-45.

10. Plumptre, C. D., Eijkelkamp, B. A., Morey, J. R., Behr, F., Couñago, R. M., Ogunniyi, A. D., Kobe, B., O'Mara, M. L., Paton, J. C. & McDevitt, C. A. J. M. m. (2014) AdcA and AdcAII employ distinct zinc acquisition mechanisms and contribute additively to zinc homeostasis in S treptococcus pneumoniae. **91**, 834-851.

11. Riordan, J. R. (2008) CFTR function and prospects for therapy, *Annu Rev Biochem.* **77**, 701-26.

12. Teague, S. J. J. N. r. D. d. (2003) Implications of protein flexibility for drug discovery. **2**, 527-541.

13. Majumder, P., Mallela, A. K. & Penmatsa, A. J. J. o. t. I. I. o. S. (2018) Transporters Through the Looking Glass: An Insight into the Mechanisms of Ion-Coupled Transport and Methods That Help Reveal Them. **98**, 283-300.

14. Majumdar, D. S., Smirnova, I., Kasho, V., Nir, E., Kong, X., Weiss, S. & Kaback, H. R. (2007) Single-molecule FRET reveals sugar-induced conformational dynamics in LacY, *Proc Natl Acad Sci U S A.* **104**, 12640-5.

15. Zhao, Y., Terry, D., Shi, L., Weinstein, H., Blanchard, S. C. & Javitch, J. A. (2010) Single-molecule dynamics of gating in a neurotransmitter transporter homologue, *Nature.* **465**, 188-93.

16. Zhao, Y., Terry, D. S., Shi, L., Quick, M., Weinstein, H., Blanchard, S. C. & Javitch, J. A. (2011) Substrate-modulated gating dynamics in a Na+-coupled neurotransmitter transporter homologue, *Nature.* **474**, 109-13.

17. Akyuz, N., Altman, R. B., Blanchard, S. C. & Boudker, O. (2013) Transport dynamics in a glutamate transporter homologue, *Nature.* **502**, 114-8.

18. Erkens, G. B., Hanelt, I., Goudsmits, J. M., Slotboom, D. J. & van Oijen, A. M. (2013) Unsynchronised subunit motion in single trimeric sodium-coupled aspartate transporters, *Nature.* **502**, 119-23.

19. Gouridis, G., Schuurman-Wolters, G. K., Ploetz, E., Husada, F., Vietrov, R., de Boer, M., Cordes, T. & Poolman, B. (2015) Conformational dynamics in substrate-binding domains influences transport in the ABC importer GlnPQ, *Nat Struct Mol Biol.* **22**, 57-64.

20. van der Velde, J. H., Oelerich, J., Huang, J., Smit, J. H., Aminian Jazi, A., Galiani, S., Kolmakov, K., Guoridis, G., Eggeling, C., Herrmann, A., Roelfes, G. & Cordes, T. (2016) A simple and versatile design concept for fluorophore derivatives with intramolecular photostabilization, *Nat Commun.* **7**, 10144.

21. de Boer, M., Gouridis, G., Vietrov, R., Begg, S. L., Schuurman-Wolters, G. K., Husada, F., Eleftheriadis, N., Poolman, B., McDevitt, C. A. & Cordes, T. (2019) Conformational and dynamic plasticity in substrate-binding proteins underlies selective transport in ABC importers, *Elife.* **8**, e44652.

22. Jazi, A. A., Ploetz, E., Arizki, M., Dhandayuthapani, B., Waclawska, I., Krämer, R., Ziegler, C. & Cordes, T. J. B. (2017) Caging and Photoactivation in Single-Molecule Förster Resonance Energy Transfer Experiments. **56**, 2031-2041.

23. Husada, F., Bountra, K., Tassis, K., de Boer, M., Romano, M., Rebuffat, S., Beis, K. & Cordes, T. J. T. E. j. (2018) Conformational dynamics of the ABC transporter McjD seen by single-molecule FRET. **37**, e100056.

24. Yang, M., Livnat Levanon, N., Acar, B., Aykac Fas, B., Masrati, G., Rose, J., Ben-Tal, N., Haliloglu, T., Zhao, Y. & Lewinson, O. (2018) Single-molecule probing of the conformational homogeneity of the ABC transporter BtuCD, *Nat Chem Biol.* **14**, 715-722.

25. Liu, Y., Liu, Y., He, L., Zhao, Y. & Zhang, X. C. J. B. R. (2018) Single-molecule fluorescence studies on the conformational change of the ABC transporter MsbA. **4**, 153-165.

26. Ha, T., Enderle, T., Ogletree, D., Chemla, D. S., Selvin, P. R. & Weiss, S. J. P. o. t. N. A. o. S. (1996) Probing the interaction between two single molecules: fluorescence resonance energy transfer between a single donor and a single acceptor. **93**, 6264-6268.

27. Ha, T. J. S. M. (2001) Single-Molecule FRET. **2**, 283-284.

28. Lerner, E., Cordes, T., Ingargiola, A., Alhadid, Y., Chung, S., Michalet, X. & Weiss, S. J. S. (2018) Toward dynamic structural biology: Two decades of single-molecule Förster resonance energy transfer. **359**.

29. Muschielok, A., Andrecka, J., Jawhari, A., Bruckner, F., Cramer, P. & Michaelis, J. (2008) A nano-positioning system for macromolecular structural analysis, *Nat Methods.* **5**, 965-71.

30. Kalinin, S., Peulen, T., Sindbert, S., Rothwell, P. J., Berger, S., Restle, T., Goody, R. S., Gohlke, H. & Seidel, C. A. (2012) A toolkit and benchmark study for FRET-restrained high-precision structural modeling, *Nat Methods.* **9**, 1218-25.

31. Hellenkamp, B., Schmid, S., Doroshenko, O., Opanasyuk, O., Kühnemuth, R., Adariani, S. R., Ambrose, B., Aznauryan, M., Barth, A. & Birkedal, V. J. N. m. (2018) Precision and accuracy of single-molecule FRET measurements—a multi-laboratory benchmark study. **15**, 669-676.

32. Cordes, T., Santoso, Y., Tomescu, A. I., Gryte, K., Hwang, L. C., Camará, B., Wigneshweraraj, S. & Kapanidis, A. N. J. B. (2010) Sensing DNA opening in transcription using quenchable Forster resonance energy transfer. **49**, 9171-9180.

33. Kapanidis, A. N., Lee, N. K., Laurence, T. A., Doose, S., Margeat, E. & Weiss, S. (2004) Fluorescence-aided molecule sorting: analysis of structure and interactions by alternating-laser excitation of single molecules, *Proc Natl Acad Sci U S A.* **101**, 8936-41.

34. Robb, N. C., Cordes, T., Hwang, L. C., Gryte, K., Duchi, D., Craggs, T. D., Santoso, Y., Weiss, S., Ebright, R. H. & Kapanidis, A. N. J. J. o. m. b. (2013) The transcription bubble of the RNA polymerase–promoter open complex exhibits conformational heterogeneity and millisecond-scale dynamics: implications for transcription start-site selection. **425**, 875-885.

35. Gouridis, G., Hetzert, B., Kiosze-Becker, K., de Boer, M., Heinemann, H., Nurenberg-Goloub, E., Cordes, T. & Tampe, R. (2019) ABCE1 Controls Ribosome Recycling by an Asymmetric Dynamic Conformational Equilibrium, *Cell Rep.* **28**, 723-734 e6.

36. Goudsmits, J. M., Slotboom, D. J. & van Oijen, A. M. J. N. c. (2017) Single-molecule visualization of conformational changes and substrate transport in the vitamin B 12 ABC importer BtuCD-F. **8**, 1-10.

37. Ruan, Y., Miyagi, A., Wang, X., Chami, M., Boudker, O. & Scheuring, S. (2017) Direct visualization of glutamate transporter elevator mechanism by high-speed AFM, *Proc Natl Acad Sci U S A.* **114**, 1584-1588.

38. Joseph, B., Sikora, A., Bordignon, E., Jeschke, G., Cafiso, D. S. & Prisner, T. F. J. A. C. (2015) Distance measurement on an endogenous membrane transporter in E. coli cells and native membranes using EPR spectroscopy. **127**, 6294-6297.

39. Sahu, I. D., McCarrick, R. M., Troxel, K. R., Zhang, R., Smith, H. J., Dunagan, M. M., Swartz, M. S., Rajan, P. V., Kroncke, B. M. & Sanders, C. R. J. B. (2013) DEER EPR measurements for membrane protein structures via bifunctional spin labels and lipodisq nanoparticles. **52**, 6627-6632.

40. Karasawa, A., Swier, L. J., Stuart, M. C., Brouwers, J., Helms, B. & Poolman, B. (2013) Physicochemical factors controlling the activity and energy coupling of an ionic strength-gated ATP-binding cassette (ABC) transporter, *J Biol Chem.* **288**, 29862-71.

41. Biemans-Oldehinkel, E., Mahmood, N. A. & Poolman, B. (2006) A sensor for intracellular ionic strength, *Proc Natl Acad Sci U S A.* **103**, 10624-9.

42. Patzlaff, J. S., van der Heide, T. & Poolman, B. (2003) The ATP/substrate stoichiometry of the ATP-binding cassette (ABC) transporter OpuA, *J Biol Chem.* **278**, 29546-51.

43. van der Heide, T., Stuart, M. C. & Poolman, B. (2001) On the osmotic signal and osmosensing mechanism of an ABC transport system for glycine betaine, *EMBO J.* **20**, 7022-32.

44. de Boer, M., Gouridis, G., Muthahari, Y. A. & Cordes, T. J. B. j. (2019) Single-molecule observation of ligand binding and conformational changes in FeuA. **117**, 1642-1654.

45. Karasawa, A., Erkens, G. B., Berntsson, R. P., Otten, R., Schuurman-Wolters, G. K., Mulder, F. A. & Poolman, B. (2011) Cystathionine beta-synthase (CBS) domains 1 and 2 fulfill different roles in ionic strength sensing of the ATP-binding cassette (ABC) transporter OpuA, *J Biol Chem.* **286**, 37280-91.

46. Kijac, A., Shih, A. Y., Nieuwkoop, A. J., Schulten, K., Sligar, S. G. & Rienstra, C. M. J. B. (2010) Lipid− protein correlations in nanoscale phospholipid bilayers determined by solid-state nuclear magnetic resonance. **49**, 9190-9198.

47. ter Beek, J., Guskov, A. & Slotboom, D. J. (2014) Structural diversity of ABC transporters, *J Gen Physiol.* **143**, 419-35.

48. Le Reste, L., Hohlbein, J., Gryte, K. & Kapanidis, A. N. J. B. j. (2012) Characterization of dark quencher chromophores as nonfluorescent acceptors for single-molecule FRET. **102**, 2658-2668.

49. Ploetz, E., Lerner, E., Husada, F., Roelfs, M., Chung, S., Hohlbein, J., Weiss, S. & Cordes, T. J. S. r. (2016) Förster resonance energy transfer and protein-induced fluorescence enhancement as synergetic multi-scale molecular rulers. **6**, 33257.

50. Bertoni, M., Kiefer, F., Biasini, M., Bordoli, L. & Schwede, T. J. S. r. (2017) Modeling protein quaternary structure of homo-and hetero-oligomers beyond binary interactions by homology. **7**, 1-15.

51. Guex, N., Peitsch, M. C. & Schwede, T. J. E. (2009) Automated comparative protein structure modeling with SWISS-MODEL and Swiss-PdbViewer: A historical perspective. **30**, S162-S173.

52. Häusler, E., Fredriksson, K., Goba, I., Peters, C., Raltchev, K., Sperl, L., Steiner, A., Weinkauf, S. & Hagn, F. J. B. e. B. A.-B. (2020) Quantifying the insertion of membrane proteins into lipid bilayer nanodiscs using a fusion protein strategy. **1862**, 183190.

53. Lewinson, O. & Livnat-Levanon, N. J. J. o. m. b. (2017) Mechanism of action of ABC importers: conservation, divergence, and physiological adaptations. **429**, 606-619.

54. Szöllősi, D., Rose-Sperling, D., Hellmich, U. A. & Stockner, T. J. B. e. B. A.-B. (2018) Comparison of mechanistic transport cycle models of ABC exporters. **1860**, 818-832.

55. Scheepers, G. H., Lycklama a Nijeholt, J. A. & Poolman, B. J. F. l. (2016) An updated structural classification of substrate-binding proteins. **590**, 4393-4401.

56. Davidson, A. L., Shuman, H. A. & Nikaido, H. J. P. o. t. N. A. o. S. (1992) Mechanism of maltose transport in Escherichia coli: transmembrane signaling by periplasmic binding proteins. **89**, 2360-2364.

57. Borths, E. L., Poolman, B., Hvorup, R. N., Locher, K. P. & Rees, D. C. J. B. (2005) In vitro functional characterization of BtuCD-F, the Escherichia coli ABC transporter for vitamin B12 uptake. **44**, 16301-16309.

58. Vigonsky, E., Ovcharenko, E. & Lewinson, O. J. P. o. t. N. A. o. S. (2013) Two molybdate/tungstate ABC transporters that interact very differently with their substrate binding proteins. **110**, 5440-5445.

59. Gul, N., Schuurman-Wolters, G., Karasawa, A. & Poolman, B. J. B. (2012) Functional characterization of amphipathic α-helix in the osmoregulatory ABC transporter OpuA. **51**, 5142-5152.

60. DeLano, W. L. J. C. N. o. p. c. (2002) Pymol: An open-source molecular graphics tool. **40**, 82-92.

61. van der Velde, J. H., Ploetz, E., Hiermaier, M., Oelerich, J., de Vries, J. W., Roelfes, G. & Cordes, T. J. C. (2013) Mechanism of intramolecular photostabilization in self-healing cyanine fluorophores. **14**, 4084-4093.

62. Rabiner, L. R. (1990) A tutorial on hidden markov models and selected applications in speech recognition. Readings in Speech Recognition (pp. 267–296) in, Los Altos, CA: Morgan Kaufmann,

Supporting information

Single-molecule studies of conformational states and dynamics in the ABC importer OpuA"

Content: Additional data and SI Note on homology modelling

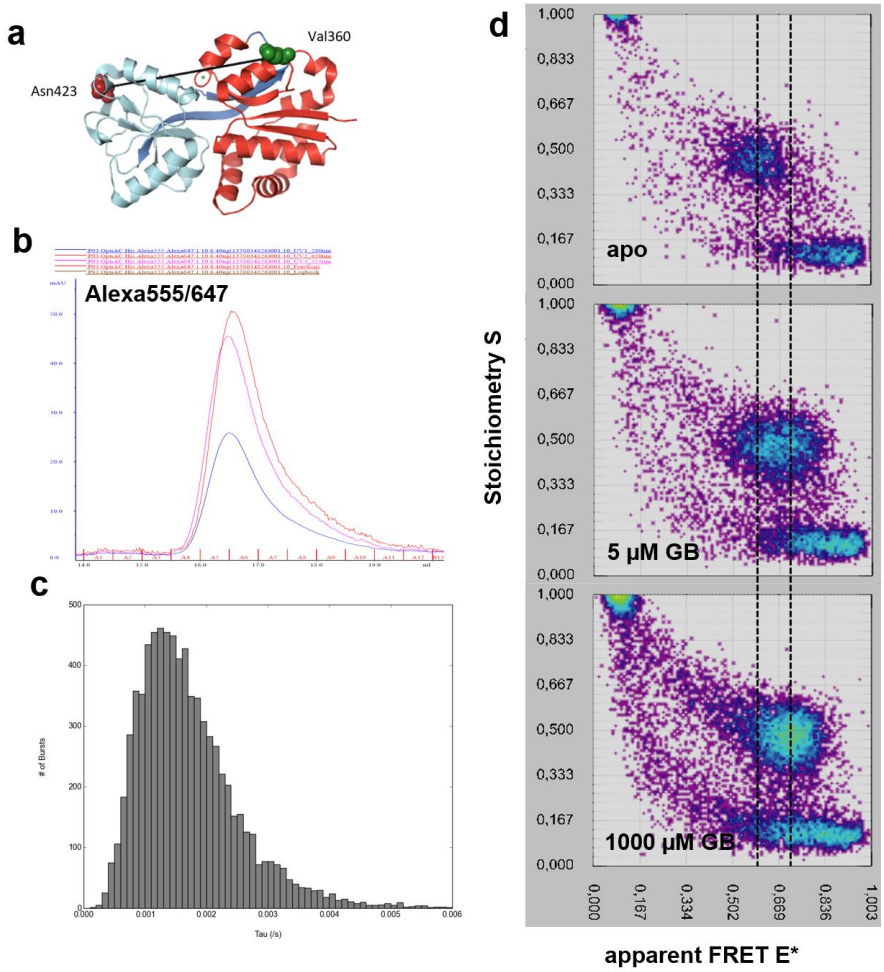

Figure S1. General description of smFRET experiments and analysis on the example of OpuAC (V360C/N423C). (a) Cartoon representation of OpuAC based on 3L6G. Residues mutated to cysteines are indicated with spheres. The two rigid domains are indicated with cyan or red color, whereas the hinge (two β strands) is shown in blue color. **(b)** After labelling with Alexa 555 and Alexa 647, OpuAC (V360C/N423C) was subjected to size exclusion chromatography, while at the same time the absorbance was monitored at three wavelengths (280 nm = blue, 555 nm = cyan, 647 nm = red) to derive labeling efficiencies. **(c/d)** Fraction A6 (eluting at ~16,7 ml, panel **(b)** was subjected to smFRET ALEX experiments, from which the burst length distribution was derived (c). The number of bursts (y axis) were plotted as a function of burst duration (x axis). **(d)** 2D ALEX histograms of single molecules (each dot is representing one labeled OpuAC (V360C/N423C) molecule which has been detected in the confocal spot) are sorted depending on their Stoichiometry. Donor-only molecules have high S > 0.8 with low E < 0.2, acceptor-only molecules of OpuAC are characterized by low S < 0.3 and widespread E. Donor-acceptor bearing OpuAC molecules lie in between both S-regimes 0.8 > S > 0.3 with characteristic E-distributions. This S-region is the selected for data representation in the main text figures in the 1D-E*-histograms. Panel **(d)** shows the FRET-efficiency shifts of OpuAC upon addition of its natural ligand glycine betaine, GB (apo = no ligand). The population of molecules is shifting from the low FRET apo condition to the high FRET fully saturating (1000 µM of glycine betaine) conditions as indicated. For data analysis in panel **(d)** an all photon burst-search was used (M = 15, T = 500 µs and L = 50) with additional thresholding of all photons >250.

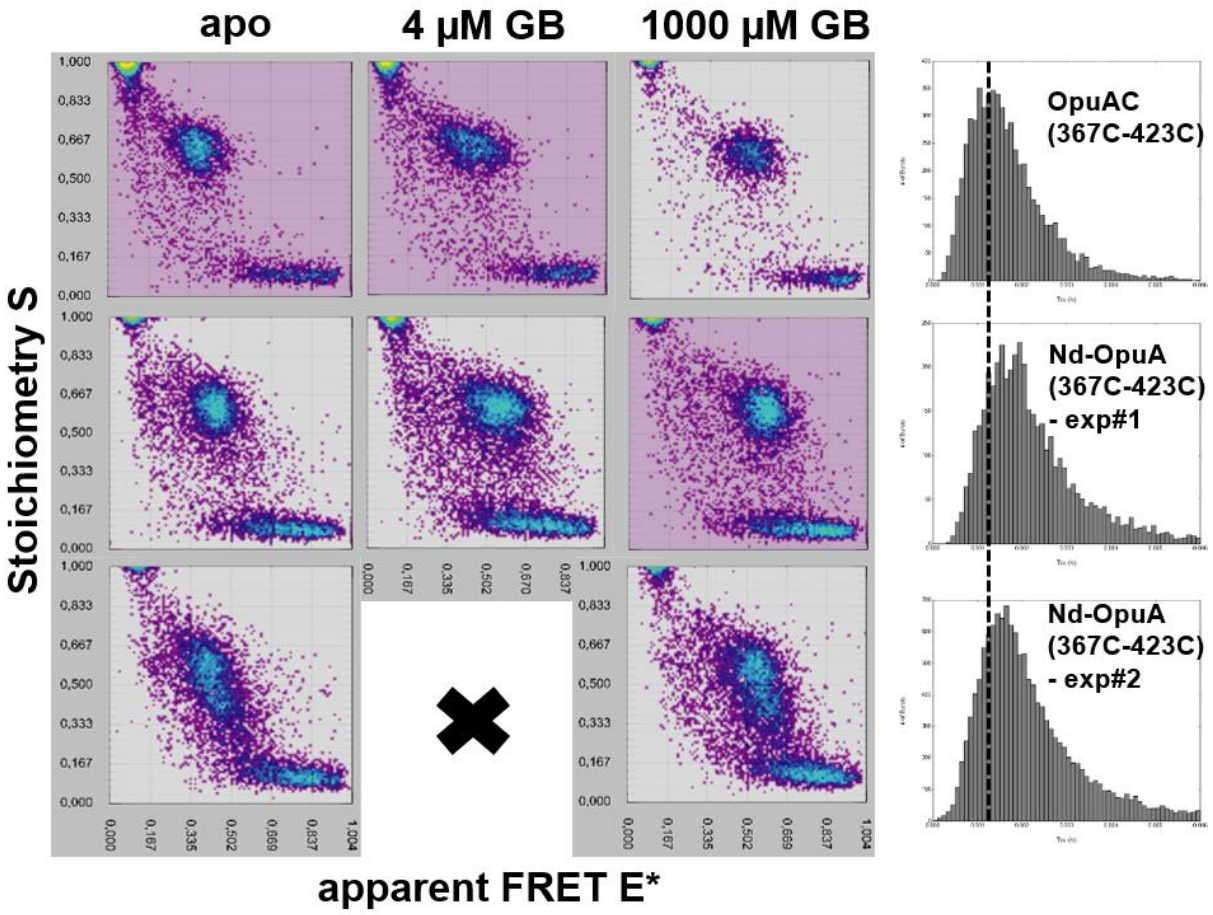

Figure S2. ALEX 2D plots (as in Supplementary Figure 1) of soluble OpuAC (OpuAC 367C/423C) or nanodisc reconstituted Nd-OpuA (367C/423C) labelled with Cy3B and ATTO647N fluorophores. The corresponding burst length distributions are indicated in the right part of the figure. The experiments were accomplished at apo protein, intermediate or saturating conditions of glycine betaine (GB). Free OpuAC has a narrow range of stoichiometry values 0.8 > S > 0.5, indicative of single proteins carrying one pair of single donor and a single acceptor fluorophore. A functional OpuA (Nd-OpuA (367C/423C)) consists of two OpuAC 367C/423C domains, thus four labeling positions are available per nanodisc complex. For this reason, the population in the nanodisc reconstituted OpuA has a wider S range 0.8 > S > 0.2. This is seen in different experiments with different labelling ratios of donor-acceptor and different degree of labelling (exp#1/exp2). Moreover, the burst length distribution in the nanodisc-reconstituted OpuA shifts towards higher values, indicative of a slower diffusion. In Figure S3, we tried to separate the population of molecules having only one OpuAC labelled per reconstituted transporter, from the molecules having more labels attached on both OpuAC. Importantly, the ligand binding is coupled to changes in FRET efficiency in all cases as found for undisturbed OpuAC (top row and data in the main text in Figure 2/3). For data analysis an all photon burst-search was used (M = 15, T = 500 µs and L = 50) with additional thresholding of all photons >250.

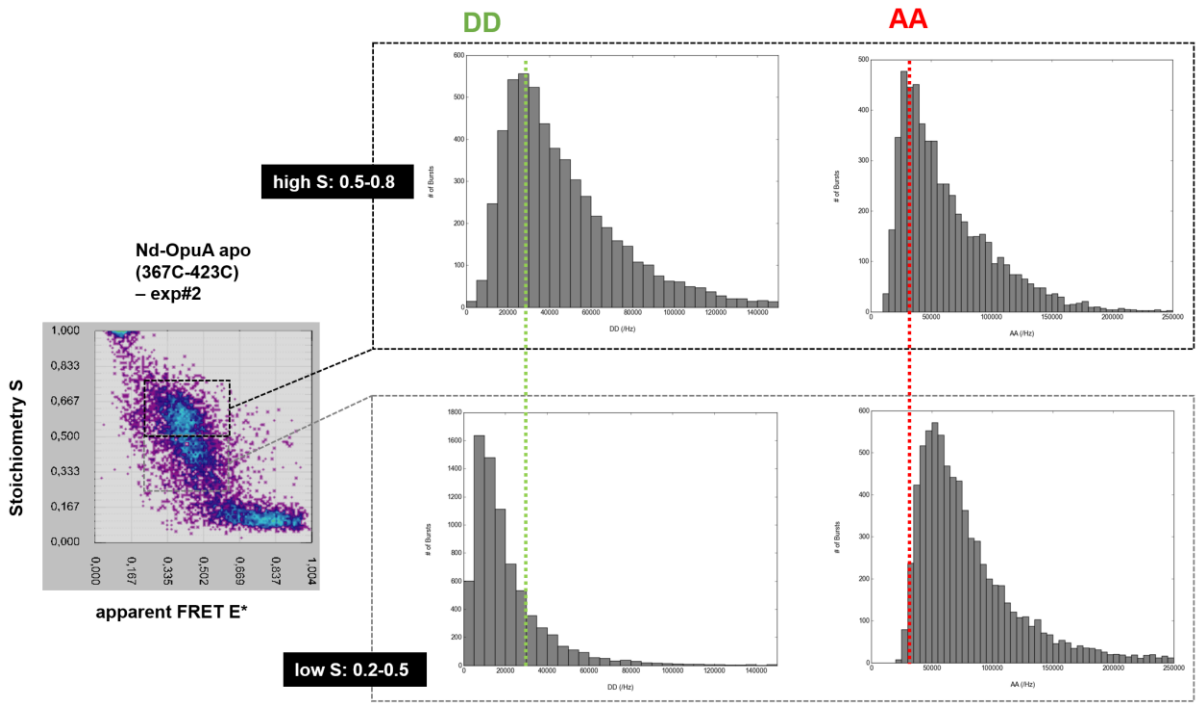

Figure S3. Analysis of the labelling composition of Nd-OpuA complexes. The figure shows burst-length normalized frequency of photon-count rates of donor-based donor emission (DD) and acceptor-based acceptor emission (AA). The correlation between S range (low/high as indicated) shows an increasing degree of fluorophores within the the Nd-OpuA complex. This is seen by increased mean AA-values (indicative of >1 acceptor dye) with concomitant decrease of DD-signal due to quenching via e.g., FRET. It is seen in comparison with Figure S2 that still the intermediate S-population carries useful information on the donor-acceptor distance for high S-values > 0.5 which has been used for analysis of all data sets shown in the main text (Figure 2,3,5). For data analysis an all photon burst-search was used (M = 15, T = 500 µs and L = 50) with additional thresholding of all photons >250.

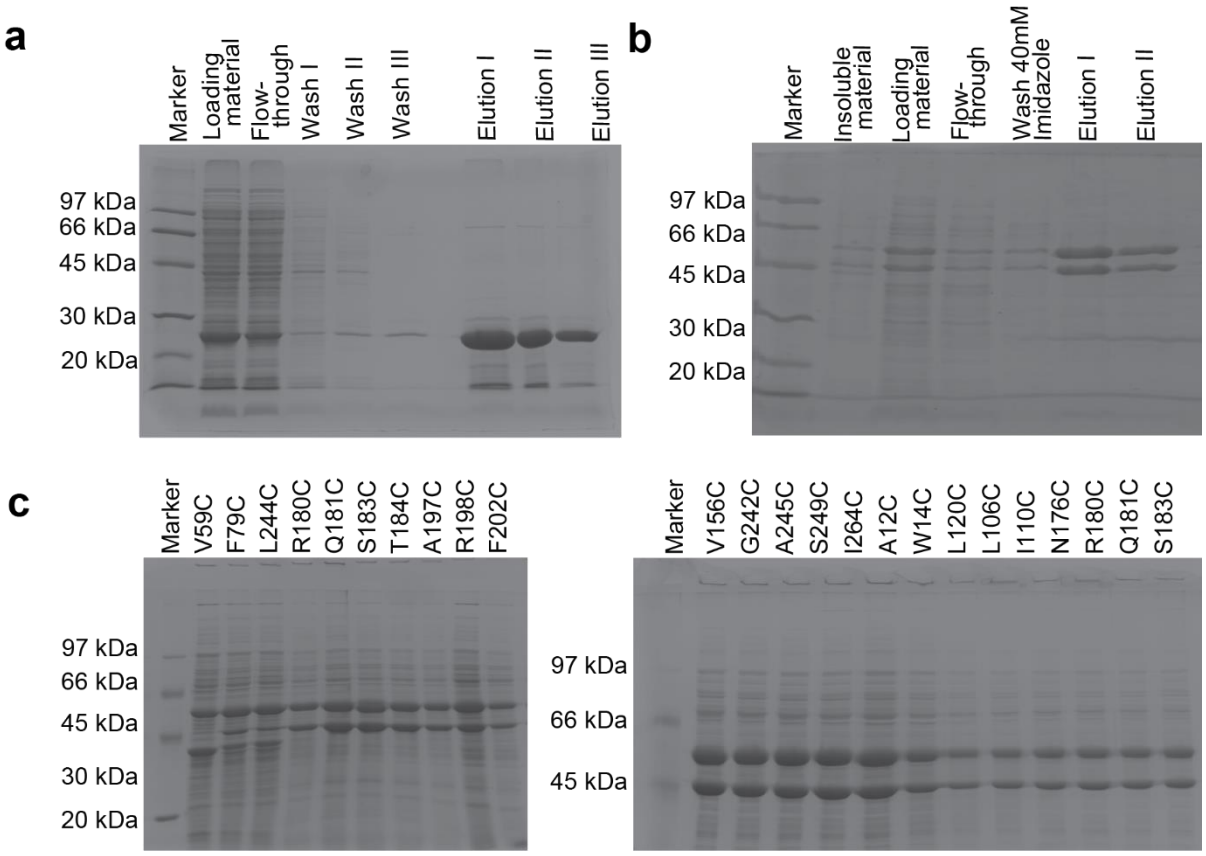

Figure S4. OpuA and MSP1D1 expression and purification. (a) SDS-PAGE from the purification of belt protein MSP_1D_1. At ~24 kDa **(b)** SDS-PAGE from purification of OpuA. **(c)** SDS-PAA gel electrophoresis of isolated membrane vesicles with overexpressed cysteine derivatives of OpuA. The mutants show high overexpression (OpuABC at 62KDa and OpuAA at 45 kDa) and in most cases equal ratio of ABC/AA subunits.

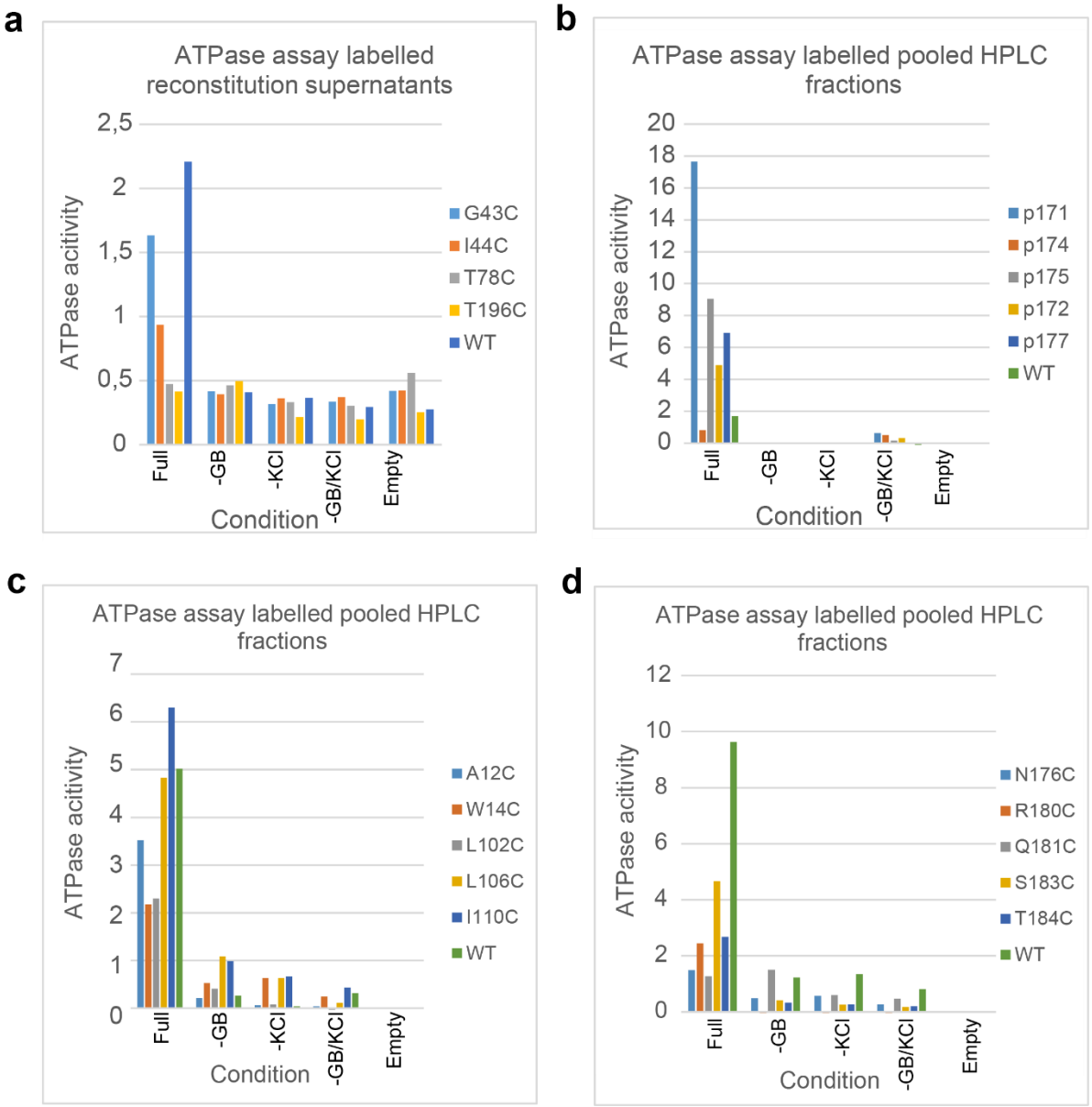

Figure S5. In vitro ATPase results. **(a)** This set of experiments was done without size exclusion chromatography of the reconstituted labeled nanodiscs. **(b/c/d)** These sets of assays were done with pooled fractions of nanodiscs purified with size exclusion chromatography. To determine the in vitro activity of the OpuA cysteine derivatives we used a coupled-enzyme ATPase assay (materials and methods). OpuA has been shown to be sensitive to ionic strength (4/37). To calculate the relative activity compared to WT, control reactions were done also in the absence of substrate (glycine betaine), salt (potassium chloride) and both a substrate and salt. Lastly a control with empty nanodiscs was done (only lipids and MSP1D1 present during reconstitution) to determine the baseline contribution of the nanodisc components to the assay. The ATPase assay was done as a quick way to screen through the library of mutants of valid candidates, therefore each mutant was tested once and the activity was calculated as the relative activity and not an absolute rate.

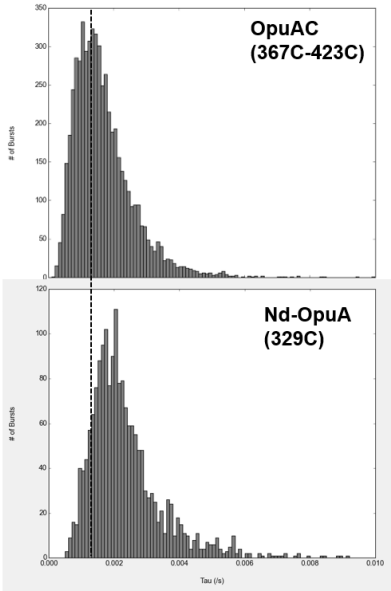

Figure S6: Burst length distributions (all 100, 0.4-0.8 S) for OpuAC (free substrate protein) and Nd-OpuA (full transporter reconstituted in nanodiscs).

Supplementary Note: Homology model.

The lack of a crystal structure for OpuA (TMD/NBD) led us to the use of homology modeling (Figure S7) as a tool to predict the position of amino acids in three-dimensional space. For successful fluorophore labeling, information such as solvent accessibility, steric hindrance and avoidance of proximity to the translocation channel were critical. Four structures were selected to serve as templates (Table S1) based on their transporter family, functionality, availability and sequence identity/similarity.

For each template an OpuA structure was predicted and all resulting models were quite similar with minor differences in loops connecting the trans-membrane helices (Figure S7). To assess the distance between target residues for mutagenesis and fluorophore labelling, we used the maltose transporter as template, because we had information on both inward (PDB: 2r6g) and outward (PDB: 3fh6) facing conformations. The transmembrane domains of the maltose transporter showed little variation in the inward and outward conformation (Figure 7) and were behaving as rigid domains. The produced inward and outward facing models were the basis for calculating the distance change between inward and outward conformations (Figure 7c/d). The relative distance change is critical information to maximize the resolution of the smFRET experiments.

The homology model we produced here is sensitive to the input template structures and with more template structures of high sequence identity it would produce more reliable results[1, 2]. The lack of solved transporter structures related to OpuA was thus limiting the accuracy/correctness of the produced model. To increase the likelihood of obtaining a functional mutant with good labelling behavior, the homology model was complemented with information on the conservation scores for all the amino acids in OpuA. This limited reliability led to consider an approach where we increase the number of the cysteine mutants in our library for testing (Figure 7a).

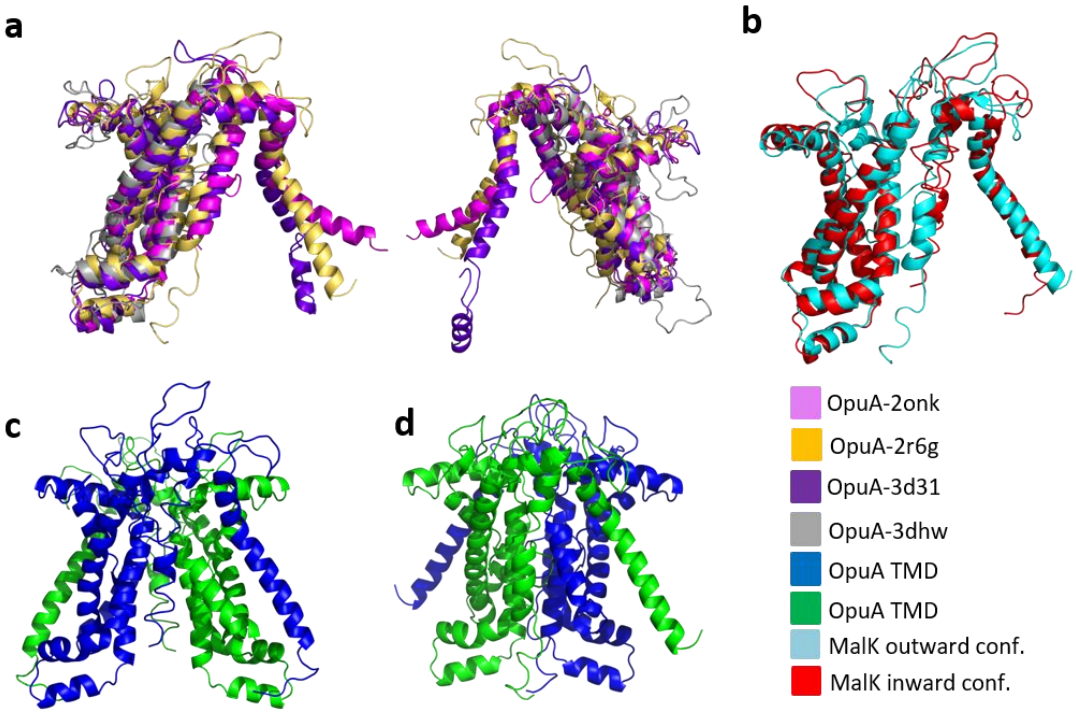

Figure S7. The homology model of the OpuA transmembrane domain was done using Swiss-model server [3]. The modelled structures were visualized using PyMol[4]. To further asses the quality of the model the modelled structures were aligned and overlaid on the template structures using PyMol. **(a)** Superimposition of the four modeled inward homology models based on the maltose, tungstate/molybdate, sulfate/molybdate and methionine importers. **(b)** Aligned transmembrane domains of the maltose importer in the outward and inward conformation. **(c)** Recreation of the TMD dimer in the inward

facing conformation using as building blocks the X-Ray structure of the maltose-based homology model of OpuA. The orientation of the dimer is with the upper plane facing the periplasm and the lower plain facing the cytoplasm. **(d)** Recreation of the TMD dimer in the outward facing conformation based on the outward facing conformation of the maltose transporter.

Table S1. List of crystal structures used as templates for OpuA-TMD. The sequence identity and similarity were calculated using protein Blast. The sequence coverage score was given by swiss model and represents the percentage of the template structure that was used for the prediction of the modeled OpuA TMD. Multiple sequence alignment was done using ClustalΩ[5].

Template	Sequence identity	Sequence similarity	Coverage	Description
2onk.1.C	24%	30%	81%	Molybdate/tungstate ABC transporter, permease protein
2r6g.1.E	20%	28%	92%	Maltose transport system permease protein MalG (inward)
4jbw.2.B	20%	28%	92%	Maltose transport system permease protein MalG (outward)
3d31.1.C	26%	29%	84%	Sulfate/molybdate ABC transporter, permease protein
3dhw.2.A	23%	32%	68%	D-methionine transport system permease protein metI

Table S2. Calculated distances between the cysteine positions in the homodimer of OpuA. The first distance is the relative distance change between the modeled inward- and outward-facing conformation. The second value represents the lower distance measured in either conformation. The maximum distance between the two fluorophores can be calculated by adding the relative distance change to the listed (minimum) distance. Conservation denotes the conservation index for each residue as calculated through ConSurf[6-11]. Due to the resolution range of smFRET low initial distances (less than 20Å) cannot be easily measured. However, they open the possibility of quenching assays as they are more sensitive for probes at close proximity.

Periplasmic			Cytoplasmic		
Mutant	**net dif. / low dist. Å**	**Conservation score**	**Mutant**	**net dif. / low dist. Å**	**Conservation score**
Gly 43 Cys	6.4 / 48.4 outw	1	**Ala 12**	10.7 / 61.8 outw	6
Ile 44 Cys	14.2 / 43.9 outw	1	**Try 14**	10.0 / 54.7 outw	2
Val 59 Cys	NA / NA	1	**Leu 102**	8.4 / 24.5 outw	4
Val 60 Cys	NA / NA	1	**Leu 106**	10.5 / 25.9 outw	1
Thr 78 Cys	7.5 / 38.9 inw	1	**Ile 110**	8.3 / 27.8 outw	1
Phe 79 Cys	6.1 / 39.1 inw	5	**Asn 176**	8.3 / 14.7 outw	7
Val 156 Cys	6.7 / 35.8 inw	7	**Arg 180**	10.0 / 13.0 outw	7
Gly 242 Cys	5.4 / 38.7 inw	5	**Gln 181**	9.7 / 9.2 outw	8
Leu 244 Cys	14.1 / 29.4 inw	8	**Ser 183**	14.4 / 9.6 outw	7
Ala 245 Cys	7.9 / 29.7 inw	6	**Thr 184**	12.4 / 15.9 outw	1
Ser 249 Cys	5.9 / 37.2 inw	7	**Thr 196**	12.3 / 44.3 outw	7
Ile 260 Cys	8.7 / 22.6 inw	3	**Ala 197**	13.1 / 42.3 outw	2
Ile 264 Cys	10.6 / 15.6 outw	7	**Arg 198**	128 / 41.0 outw	1
Phe 202	13.7 / 33.6 outw	1			

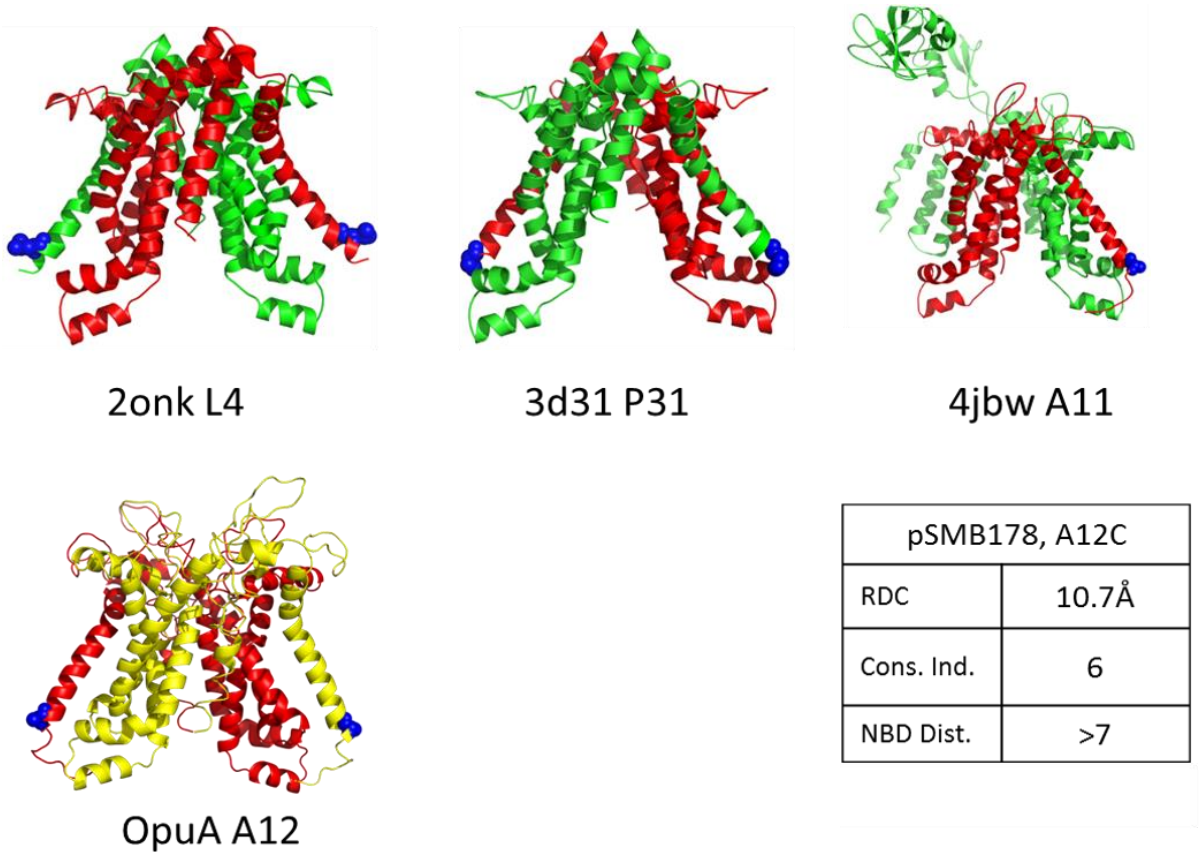

pSMB178, A12C	
RDC	10.7Å
Cons. Ind.	6
NBD Dist.	>7

Figure S8. OpuA homology models with selected labelling positions relevant to monitoring TMD movements. OpuA A12C modelled inward facing dimer (OpuA A12) in red/yellow. The rest are the structures of the three templates (2onk Molybdate/tungstate ABC transporter, 3d31 Sulfate/molybdate ABC transporter, 4jbw MalG). With blue spheres are denoted the homologous amino acids to the Alanine 12 of OpuA as determined from multiple amino acid sequence alignment using ClustalW (the four template amino acid sequences were aligned with the sequence of OpuA). All the cartoons are oriented the same way, with the periplasmic space being above the cartoon and the cytoplasmic below. The cell membrane is perpendicular to the plane of the screen/paper. All the cartoons are in the inward facing conformation. RDC is realtive distance change between tha inear and outward facing conformation for Ala12. Conservation index is the conseravation score of Ala12 as calculated by ConSurf (1 being least conserved, 10 being most conserved. NBD distance is the expected distance of the Ala12 form the nucleotide binding domain based on the model (close proximity to the NBD could impair activity).

Table S3. QC-PCR primers for cysteine derivatives of OpuA

X001	5' GTTGACTTAGTTTATATGTGTTGGGATTCAGAAGTTGCA 3'	Fw Asn329Cys SBD OpuAC
X002	5' TGCAACTTCTGAATCCCA**ACA**CATATAAACTAAGTCAAC 3'	Rev Asn329Cys SBD OpuAC
X013	5' TGGCAAACAGTAGCC**TGT**GGTCAAGCAGATGGA 3'	Fw Asn367 SBD OpuAC
X014	5' TCCATCTGCTTGACC**ACA**GGCTACTGTTTG CCA 3'	Rev Asn367 SBD OpuAC
X017	5' TCAATTGAAGATTTAACA**TGT**CAAGCGAATAAAACAATC 3'	Fw Asn423Cys SBD OpuAC
X018	5' GATTGTTTTATTCGCTTG**ACA**TGTTAAATCTTCAATTGA 3'	Rev Asn423Cys SBD OpuAC
X066	5' ACAGCTTTAGATAATGCG**TGT**GCTTGGCAAACAGTAGCC 3'	Fw Val360Cys SBD OpuAC
X067	5' GGCTACTGTTTGCCAAGC**ACA**CGCATTATCTAAAGCTGT 3'	Rev Val360Cys SBD OpuAC
X117	5'GGAACGGTATTGATGAAC**TGT**ATTACAGGTGCTTTAACT3'	Fw Gly43Cys TMD OpuA
X118	5'AGTTAAAGCACCTGTAAT**ACA**GTTCATCAATACCGTTCC3'	Rev Gly43Cys TMD OpuA
X119	5'ACGGTATTGATGAACGGT**TGT**ACAGGTGCTTTAACTGCT3'	Fw Ile44Cys TMD OpuA
X120	5'AGCAGTTAAAGCACCTGT**ACA**ACCGTTCATCAATACCGT3'	Rev Ile44Cys TMD OpuA

X121	5’TTCTGGTTGATGATTGCT**TGT**GTTACTATCCTTGCCATT3’	Fw Val59Cys	TMD OpuA
X122	5’AATGGCAAGGATAGTAAC**ACA**AGCAATCATCAACCAGAA3’	Rev Val59Cys	TMD OpuA
X123	5’TGGTTGATGATTGCTGTT**TGT**ACTATCCTTGCCATTTTG3’	Fw Val60Cys	TMD OpuA
X124	5’CAAAATGGCAAGGATAGT**ACA**AACAGCAATCATCAACCA3’	Rev Val60Cys	TMD OpuA
X125	5’ATTGCCTTTCCTTTATTC**TGT**TTCATCGGTCTTTCTTTA3’	Fw Thr78Cys	TMD OpuA
X126	5’TAAAGAAAGACCGATGAA**ACA**GAATAAAGGAAAGGCAAT3’	Rev Thr78Cys	TMD OpuA
X127	5’GCCTTTCCTTTATTCACT**TGT**ATCGGTCTTTCTTTAATT3’	Fw Phe79Cys	TMD OpuA
X128	5’AATTAAAGAAAGACCGAT**ACA**AGTGAATAAAGGAAAGGC3’	Rev Phe79Cys	TMD OpuA
X129	5’GCATTCTTTGGAATAGGA**TGT**GTTCCTGGGGTATTTGCA3’	Fw Val156Cys	TMD OpuA
X130	5’TGCAAATACCCCAGGAAC**ACA**TCCTATTCCAAAGAATGC3’	Rev Val156Cys	TMD OpuA
X131	5’GCGCCTGGCTTAGGTCGT**TGT**GTACTTGCAGCTGTTCAA3’	Fw Gly242Cys	TMD OpuA
X132	5’TTGAACAGCTGCAAGTAC**ACA**ACGACCTAAGCCAGGCGC3’	Rev Gly242Cys	TMD OpuA
X133	5’GGCTTAGGTCGTGGTGTA**TGT**GCAGCTGTTCAATCGGCT3’	Fw Leu244Cys	TMD OpuA
X134	5’AGCCGATTGAACAGCTGC**ACA**TACACCACGACCTAAGCC3’	Rev Leu244Cys	TMD OpuA
X135	5’TTAGGTCGTGGTGTACTT**TGT**GCTGTTCAATCGGCTGAT3’	Fw Ala245Cys	TMD OpuA
X136	5’ATCAGCCGATTGAACAGC**ACA**AAGTACACCACGACCTAA3’	Rev Ala245Cys	TMD OpuA
X137	5’GTACTTGCAGCTGTTCAA**TGT**GCTGATATTGGTAAAGGG3’	Fw Ser249Cys	TMD OpuA
X138	5’CCCTTTACCAATATCAGC**ACA**TTGAACAGCTGCAAGTAC3’	Rev Ser249Cys	TMD OpuA
X139	5’AAAGGGTTTGTAAGTGGG**TGT**TCATTAGTTATTTTGGCT3’	Fw Ile260Cys	TMD OpuA
X140	5’AGCCAAAATAACTAATGA**ACA**CCCACTTACAAACCCTTT3’	Rev Ile260Cys	TMD OpuA
X141	5’AGTGGGATTTCATTAGTT**TGT**TTGGCTATTATTATTGAC3’	Fw Ile264Cys	TMD OpuA
X142	5’GTCAATAATAATAGCCAA**ACA**AACTAATGAAATCCCACT3’	Rev Ile264Cys	TMD OpuA
X143	5’ATTGGACAAGTACCCATA**TGT**AACTGGGTGTCATCGGCA3’	Fw Ala12Cys	TMD OpuA
X144	5’TGCCGATGACACCCAGTT**ACA**TATGGGTACTTGTCCAAT3’	Rev Ala12Cys	TMD OpuA
X145	5’CAAGTACCCATAGCAAAC**TGT**GTGTCATCGGCAACAGAT3’	Fw Trp14Cys	TMD OpuA
X146	5’ATCTGTTGCCGATGACAC**ACA**GTTTGCTATGGGTACTTG3’	Rev Trp14Cys	TMD OpuA
X147	5’AGTACAATCACACTTGTC**TGT**CTTTCAAGTTTATTGTCA3’	Fw Leu102Cys	TMD OpuA
X148	5’TGACAATAAACTTGAAAG**ACA**GACAAGTGTGATTGTACT3’	Rev Leu102Cys	TMD OpuA
X149	5’CTTGTCTTACTTTCAAGT**TGT**TTGTCAATCATCATTGGA3’	Fw Leu106Cys	TMD OpuA
X150	5’TCCAATGATGATTGACAA**ACA**ACTTGAAAGTAAGACAAG3’	Rev Leu106Cys	TMD OpuA
X151	5’TCAAGTTTATTGTCAATC**TGT**ATTGGAGTTCCTTTAGGG3’	Fw Ile110Cys	TMD OpuA
X152	5’CCCTAAAGGAACTCCAAT**ACA**GATTGACAATAAACTTGA3’	Rev Ile110Cys	TMD OpuA
X153	5’CCAACAGTCAGAATGACT**TGT**TTGGGAATTCGTCAAGTT3’	Fw Asn176Cys	TMD OpuA
X154	5’AACTTGACGAATTCCCAA**ACA**AGTCATTCTGACTGTTGG3’	Rev Asn176Cys	TMD OpuA
X155	5’ATGACTAACTTGGGAATT**TGT**CAAGTTTCAACGGAATTA3’	Fw Arg180Cys	TMD OpuA
X156	5’TAATTCCGTTGAAACTTG**ACA**AATTCCCAAGTTAGTCAT3’	Rev Arg180Cys	TMD OpuA
X157	5’ACTAACTTGGGAATTCGT**TGT**GTTTCAACGGAATTAGTT3’	Fw Gln181Cys	TMD OpuA
X158	5’AACTAATTCCGTTGAAAC**ACA**ACGAATTCCCAAGTTAGT3’	Rev Gln181Cys	TMD OpuA
X159	5’TTGGGAATTCGTCAAGTT**TGT**ACGGAATTAGTTGAAGCG3’	Fw Ser183Cys	TMD OpuA
X160	5’CGCTTCAACTAATTCCGT**ACA**AACTTGACGAATTCCCAA3’	Rev Ser183Cys	TMD OpuA
X161	5’GGAATTCGTCAAGTTTCA**TGT**GAATTAGTTGAAGCGGCA3’	Fw Thr184Cys	TMD OpuA
X162	5’TGCCGCTTCAACTAATTC**ACA**TGAAACTTGACGAATTCC3’	Rev Thr184Cys	TMD OpuA
X163	5’GCAGATTCATTTGGTTCA**TGT**GCCCGTCAAAAGCTTTTT3’	Fw Thr196Cys	TMD OpuA
X164	5’AAAAAGCTTTTGACGGGC**ACA**TGAACCAAATGAATCTGC3’	Rev Thr196Cys	TMD OpuA
X165	5’GATTCATTTGGTTCAACT**TGT**CGTCAAAAGCTTTTTAAA3’	Fw Ala197Cys	TMD OpuA
X166	5’TTTAAAAAGCTTTTGACG**ACA**AGTTGAACCAAATGAATC3’	Rev Ala197Cys	TMD OpuA
X167	5’TCATTTGGTTCAACTGCC**TGT**CAAAAGCTTTTTAAATTG3’	Fw Arg198Cys	TMD OpuA
X168	5’CAATTTAAAAAGCTTTTG**ACA**GGCAGTTGAACCAAATGA3’	Rev Arg198Cys	TMD OpuA
X169	5’ACTGCCCGTCAAAAGCTT**TGT**AAATTGGAATTTCCTTTG3’	Fw Phe202Cys	TMD OpuA
X170	5’CAAAGGAAATTCCAATTT**ACA**AAGCTTTTGACGGGCAGT3’	Rev Phe202Cys	TMD OpuA

TableS4: List of maleimide fluorophores used in this study including their extinction coefficients. Sources were company web-portals of Thermo-Fischer for AlexaFluor dyes[12], ATTOTEC[13], Lumiprobe[14] and ref. [15] for Cy3B.

Fluorophore	Extinction Coefficient
AlexaFluor 555™	155000 $cm^{-1}M^{-1}$
AlexaFluor 647™	270000 $cm^{-1}M^{-1}$
TMR	60000 $cm^{-1}M^{-1}$
Cy5	250000 $cm^{-1}M^{-1}$
Atto647N™	150000 $cm^{-1}M^{-1}$
Cy3B	130000 $cm^{-1}M^{-1}$

References

1. Bordoli, L., Kiefer, F., Arnold, K., Benkert, P., Battey, J. & Schwede, T. J. N. p. (2009) Protein structure homology modeling using SWISS-MODEL workspace. **4**, 1.

2. Schwede, T., Kopp, J., Guex, N. & Peitsch, M. C. J. N. a. r. (2003) SWISS-MODEL: an automated protein homology-modeling server. **31**, 3381-3385.

3. Guex, N., Peitsch, M. C. & Schwede, T. J. E. (2009) Automated comparative protein structure modeling with SWISS-MODEL and Swiss-PdbViewer: A historical perspective. **30**, S162-S173.

4. Delano, W. L. J. S. L. (2002) The PyMOL molecular graphics system, version 1.8. **10**.

5. Sievers, F., Wilm, A., Dineen, D., Gibson, T. J., Karplus, K., Li, W., Lopez, R., McWilliam, H., Remmert, M. & Söding, J. J. M. s. b. (2011) Fast, scalable generation of high-quality protein multiple sequence alignments using Clustal Omega. **7**, 539.

6. Ashkenazy, H., Abadi, S., Martz, E., Chay, O., Mayrose, I., Pupko, T. & Ben-Tal, N. J. N. a. r. (2016) ConSurf 2016: an improved methodology to estimate and visualize evolutionary conservation in macromolecules. **44**, W344-W350.

7. Ashkenazy, H., Erez, E., Martz, E., Pupko, T. & Ben-Tal, N. J. N. a. r. (2010) ConSurf 2010: calculating evolutionary conservation in sequence and structure of proteins and nucleic acids. **38**, W529-W533.

8. Berezin, C., Glaser, F., Rosenberg, J., Paz, I., Pupko, T., Fariselli, P., Casadio, R. & Ben-Tal, N. J. B. (2004) ConSeq: the identification of functionally and structurally important residues in protein sequences. **20**, 1322-1324.

9. Celniker, G., Nimrod, G., Ashkenazy, H., Glaser, F., Martz, E., Mayrose, I., Pupko, T. & Ben-Tal, N. J. I. J. o. C. (2013) ConSurf: using evolutionary data to raise testable hypotheses about protein function. **53**, 199-206.

10. Glaser, F., Pupko, T., Paz, I., Bell, R. E., Bechor-Shental, D., Martz, E. & Ben-Tal, N. J. B. (2003) ConSurf: identification of functional regions in proteins by surface-mapping of phylogenetic information. **19**, 163-164.

11. Landau, M., Mayrose, I., Rosenberg, Y., Glaser, F., Martz, E., Pupko, T. & Ben-Tal, N. J. N. a. r. (2005) ConSurf 2005: the projection of evolutionary conservation scores of residues on protein structures. **33**, W299-W302.

12.https://www.thermofisher.com/de/de/home/references/molecular-probes-the-handbook/technical-notes-and-product-highlights/the-alexa-fluor-dye-series.html

13. https://www.atto-tec.com/product_info.php?info=p114_atto-647n.html

14. https://de.lumiprobe.com/fluorophore-chart

15. Cooper, M., Ebner, A., Briggs, M., Burrows, M., Gardner, N., Richardson, R. & West, R. (2004) Cy3B^{TM}: Improving the Performance of Cyanine Dyes. *Journal of Fluorescence,* **14**, 145-150.